Ultrashort pulse thulium-doped fiber lasers and amplifiers

Von der Fakultät für Mathematik und Physik
der Gottfried Wilhelm Leibniz Universität Hannover
zur Erlangung des Grades

Doktor der Naturwissenschaften
Dr. rer. nat.

genehmigte Dissertation

von

Dipl.-Phys. Frithjof Haxsen
geboren am 16.12.1982 in Hannover

2013

Referent: Prof. Dr. Uwe Morgner
Korreferent: Prof. Dr. Detlev Ristau
Tag der Promotion: 06.02.2013

Abstract

The subject of this thesis is the generation and amplification of ultrashort pulses in the 2 µm spectral region based on thulium-doped silica fibers. Due to the anomalous dispersion of silica fibers in this wavelength region, previously demonstrated mode-locked thulium lasers have been restricted to operation in the fundamental soliton regime, which limits the maximum pulse energy and minimum pulse duration. In the framework of this thesis, various concepts for the scaling of the pulse energy and duration have been investigated. With these concepts, both significantly larger pulse energies as well as shorter pulse durations could be achieved.

The stretched-pulse-operation scheme enables the generation of very short pulses and relatively large pulse energies in the wavelength region around 1 and 1.5 µm. However, this regime requires a dispersion management and, thus, in the spectral region of 2 µm the implementation of normal dispersion. Via the application of a grating arrangement with a telescope stretched-pulse operation could be demonstrated in the 2 µm spectral region for the first time. With this concept, an increase of the pulse energy of more than an order of magnitude compared to previous systems could be achieved. Adaptation of the distance between the gratings enabled variation of the cavity dispersion during mode-locked laser operation.

The stretched-pulse oscillator was used as seed source for a subsequent fiber amplifier, where the concept of chirped pulse amplification was applied to thulium-doped fibers for the first time. With this concept, efficient pulse amplification and significant pulse energy scaling could be achieved while still maintaining a nearly constant pulse duration.

Furthermore, a fiber providing normal dispersion was implemented for dispersion management for the first time into a core-pumped, hybridly mode-locked thulium fiber laser and operation with a monotonically positively chirped pulse propagation scheme could be achieved. This operation regime enabled large pulse energies with still relatively short pulse durations in the spectral region of 1 and 1.5 µm. The experimental and numerical investigations revealed numerous similarities to corresponding ytterbium- and erbium-doped oscillators. Via the numerical simulations a limitation for the relatively low pulse energy could be identified and approaches for the pulse parameter scaling could be investigated.

Keywords: ultrashort pulse; thulium; fiber.

Kurzzusammenfassung

Das Thema dieser Arbeit ist die Erzeugung und Verstärkung von ultrakurzen Pulsen im Spektralbereich um 2 µm mittels Thulium-dotierter Quarzglasfasern. Aufgrund der anomalen Dispersion von Quarzglasfasern in diesem Wellenlängenbereich waren vormals demonstrierte modengekoppelte Thuliumlaser auf den Betrieb im fundamentalen Solitonen-Regime beschränkt, wodurch die maximale Pulsenergie und minimale Pulsdauer begrenzt waren. Im Rahmen dieser Arbeit wurden verschiedene Konzepte zur Skalierung der Pulsenergie und -dauer untersucht. Mithilfe dieser Konzepte konnten sowohl deutlich größere Pulsenergien als auch kürzere Pulsdauern erreicht werden.
Der Stretched-pulse-Betrieb ermöglichte im Wellenlängenbereich um 1 und 1,5 µm die Erzeugung sehr kurzer Pulse und vergleichsweise hoher Pulsenergien. Dieses Regime setzt jedoch ein Dispersionsmanagement und damit im Spektralbereich von 2 µm die Implemenierung von normaler Dispersion voraus. Durch den Einsatz eines Gitteraufbaus mit einem Teleskop konnte erstmalig ein Stretched-pulse-Betrieb im Spektralbereich um 2 µm demonstriert werden. Mit diesem Konzept wurde eine Erhöhung der Pulsenergie von über einer Größenordnung im Vergleich zu früheren Systemen erreicht. Die Anpassung des Gitterabstandes ermöglichte eine Variation der Resonatordispersion während des modengekoppelten Betriebes.
Der Stretched-pulse Oszillator wurde als Seed-Quelle für einen nachfolgenden Faserverstärker eingesetzt, bei dem das Konzept der "Chirped-pulse-amplification" erstmalig auf Thulium-dotierte Fasern angewendet wurde. Mithilfe dieses Konzeptes konnte eine effiziente Verstärkung und eine erhebliche Skalierung der Pulsenergie bei nahezu konstanter Pulsdauer erreicht werden.
Weiterhin wurde erstmalig eine Faser mit normaler Dispersion zur Dispersionsanpassung in einem kerngepumpten, hybrid-modengekoppelten Thulium-Faserlaser eingesetzt und damit ein Betrieb mit monoton positiv gechirpter Pulspropagation erreicht. Dieses Betriebsregime ermöglicht im Spektralbereich von 1 und 1,5 µm hohe Pulsenergien bei gleichzeitig relativ kurzen Pulsdauern. Die experimentellen und numerischen Untersuchungen des Systems ergaben zahlreiche Gemeinsamkeiten mit den entsprechenden Ytterbium- oder Erbium-dotierten Oszillatoren. Mithilfe der numerischen Simulationen konnte zudem die vergleichsweise geringe Pulsenergie begründet und Möglichkeiten zur Skalierung der Pulsparameter untersucht werden.
Schlagworte: Ultrakurzpuls; Thulium; Faser.

Contents

1 Introduction

Ultrashort pulse laser sources with pulse durations in the femtosecond regime are increasingly used in numerous application areas. Hereby, different properties of ultrashort pulses are useful for different applications. Pulses with high energy and durations of several 100 fs are suitable for highly precise micro-machining applications. High field applications like the generation of high harmonics benefit from the large peak intensities of ultrashort pulses. The broad spectrum can be utilized for fast spectroscopic measurements and not at least, optical frequency combs established a whole new, rapidly growing scientific area providing previously unknown precision in metrology and spectroscopy.
In the vast majority of these applications, mode-locked lasers are used as source of the ultrashort pulses. Ti:sapphire lasers have been established as workhorses for ultrashort pulse applications in a multitude of laboratories. The Ti:sapphire crystal excels by an octave-spanning amplification bandwidth around 800 nm, enabling pulse durations down to less than 10 fs. However, solid-state lasers based on crystals suffer from several drawbacks detracting broader fields of application, especially in the commercial sector. Especially for Ti:sapphire lasers, one of these drawbacks is that up to now, no satisfactory solution for diode laser pumping has been established. The typical use of frequency-doubled solid-state lasers as pump sources results in low overall efficiencies and causes high costs. High power pumping of crystal-based lasers introduces a thermal lens, which needs to be carefully adjusted to maintain a good beam quality. Their freespace setup makes crystal-based lasers furthermore sensitive to mechanical perturbation and therefore inhibits the routine application outside of laboratory environments.

In recent years, ultrashort pulse sources based on rare earth-doped optical fibers are increasingly superseding crystal-based systems in many application areas as they provide

numerous advantages due to their waveguide properties. Their excellent beam quality is determined by the fiber characteristics and thus very robust against external perturbations. Furthermore, rare-earth doped fibers can typically be pumped by diode lasers, which allows for a very simple and efficient pumping scheme. The relatively low pump absorption and signal gain can easily be compensated by long interaction distances. Also the thermal management is very simple due to the large surface to volume ratio. Not at least, the potential of all-integrated setups makes fiber lasers very robust against mechanical perturbation and thus suitable for the application in industrial environments. However, compared to their bulk counterparts, fiber lasers are inferior in terms of pulse energy and duration. Due to the large interaction distances and small mode-field areas, the fiber dispersion and nonlinearity substantially influence a pulse along the propagation, limiting the minimum pulse duration and maximum pulse energy. Consequently, the output pulse parameters of an ultrashort pulse fiber laser are mainly determined by the resonator internal pulse propagation.

Several conceptional modifications enabled significant improvement of the fiber laser pulse parameters, making them nowadays competitive with bulk lasers. In 1993, Tamura et al. demonstrated stretched-pulse operation in an erbium-doped fiber laser for the first time [1]. By implementing dispersion management into the laser cavity, a breathing pulse dynamics could be realized, which enabled significantly shorter pulse durations and an increase of the pulse energy by an order of magnitude compared to soliton operation. However, the pulse energy was still limited by the nonlinear influence either due to optical wave-breaking or to soliton compression at the position of minimum pulse duration inside the resonator. Further significant increase of the pulse energy could be achieved with operation schemes, at which the pulse was positively chirped during the entire resonator propagation. Such a scheme was experimentally demonstrated with an ytterbium-doped fiber laser by Ilday et al. in 2003 for the first time [2].

The spectral areas around 1 and 1.5 µm wavelength are covered by lasers based on Yb^{3+}- and Er^{3+}-doped fibers, respectively, which have been intensively investigated in recent years and provide pulses with up to several 10 nJ of energy and below 100 fs duration.

Tm^{3+}-doped fibers extend the accessible wavelength range towards the 2 µm spectral region with potential applications in medicine, spectroscopy, or nonlinear frequency conversion towards the mid-infrared. The broad amplification bandwidth, ranging from about 1.8 to 2.1 µm, makes them suitable for the generation of pulses with durations of less than 100 fs.

In the 2 µm wavelength region, the dispersion of silica fibers is typically anomalous. Therefore, thulium-doped fiber lasers have previously been restricted to operation in the fundamental soliton regime, which is very easy to achieve, but also limited in terms of the output pulse energy. Thus, the pulse energy of these lasers did not exceed several ten to hundred Picojoule [3, 4, 5, 6].

Larger pulse energies could be demonstrated with ultrashort pulse lasers based on thulium-doped crystals. In recent years, several oscillators based on different crystal host materials have been demonstrated, reaching maximum pulse energies of several Nanojoule and pulse durations down to several hundred femtoseconds [7, 8]. In very recent publications, a maximum pulse energy of 3.9 nJ with 549 fs pulse duration and a minimum pulse duration of 218 fs with 1.7 nJ pulse energy could be demonstrated [9, 10]. However, beside the freespace setup, making them prone to mechanical disturbances, these oscillators are pumped by Ti:sapphire lasers, which leads to an even more complex setup and a very low overall efficiency.

The aim of this work was to transfer the concepts, which enabled significant improvements of the pulse parameters of ultrashort pulse sources based ytterbium- and erbium-doped fibers, to thulium-doped systems and to investigate the potential of pulse parameter scaling. Different approaches have been studied to achieve shorter pulse durations as well as larger pulse energies compared to soliton fiber lasers. In chapter 2, the fundamental requirements and basic concepts, which are relevant in the context of ultrashort pulse thulium fiber lasers are introduced briefly. This includes some properties of thulium-doped fibers, the various effects influencing a pulse during propagation in a fiber and the resulting laser propagation schemes as well as a short overview of the

mechanisms for the pulse generation, which are relevant in the context of this work.
In chapter 3, investigations on a thulium-doped fiber laser with a grating arrangement for dispersion compensation are presented. For the first time, stretched-pulse operation could be demonstrated in a thulium-doped fiber laser. The cavity dispersion was continuously varied from positive to negative cavity dispersion. For a cavity dispersion of -0.0275 ps^2 and +0.0385 ps^2, the influence of the pump power on the output pulse parameter was representatively examined. Numerical simulations support the experimentally observed results and provided deeper insight into the operation scheme.
The pulses delivered by the laser system presented in chapter 3 were then subsequently amplified. The corresponding investigations are described in chapter 4. In section 4.1, investigations on an amplification scheme similar than previously demonstrated by Imeshev and Fermann are presented [11]. The chirp of the pulses delivered by the oscillator was overcompensated such that it became minimal at the end of the amplification fiber. With this concept, significant spectral broadening and correspondingly shortening of the pulse duration could be achieved. For further investigations, the concept of chirped pulse amplification was applied to a 2 µm ultrashort pulse system for the first time. The corresponding results are described in section 4.2. Additional chirping of the seed pulses was achieved by adding passive fiber before the amplification fiber section. After amplification, the pulses were recompressed with a grating arrangement similar to the one that was also applied inside the laser cavity.
In chapter 5, investigations on dispersion management with a normal dispersion fiber are presented. Preliminary experiments on the adaptation of the pulses of lasers operating in the fundamental soliton regime with the implementation of normal dispersion fiber are described in section 5.1. Overcompensation of the negative fiber group delay dispersion enabled mode-locked operation with a monotonically positively chirped pulse operation scheme. The corresponding results are presented in section 5.2. Numerical simulations provided deeper insight in the pulse evolution and the limitation of the pulse parameters.
Finally, in chapters 6 and 7, the results presented in this thesis are summarized and an outlook on possible future investigations is given.

2 Fundamentals

In this chapter, general fundamentals which are relevant in the context of this thesis are provided. In section 2.1, the spectral properties of thulium-doped fibers are introduced. Section 2.2 deals with physical effects, which influence an ultra-short pulse propagating in an optical fiber and the numerical modelling of pulse propagation.

2.1 Thulium-doped fibers

Optical fibers can be doped with various lanthanides, making them suitable for the generation and amplification of light in different wavelength regions, mostly in the infrared. The spectroscopic properties are mainly given by the doping, but also depend on the host glass material.

In Fig. 2.1, a simplified scheme of the optical transitions and the resulting cross sections of thulium doped silica fibers are displayed. The emission cross section extends from about 1550 to above 2200 nm with a maximum around 1850 nm. The absorption cross section is characterized by several absorption peaks at about 680, 790 and 1210 nm and a wide absorption band ranging from 1400 to 1800 nm.

In laser development, different pumping schemes utilizing different optical transitions have been established. The broad absorption band around 1630 nm can be addressed with single-mode pump sources based on erbium-doped fibers to directly excite $^3H_4$ level (see Fig. 2.1 (a)). These pump sources can easily reach several 100 mW to several Watt of output power at wavelengths around 1550 nm, which then can be delivered into the core of the active fiber via a wavelength division multiplexer (WDM) enabling several 10 to 100 mW of average output power at 2 µm.

In order to achieve larger output power levels, fiber-coupled diode lasers with several

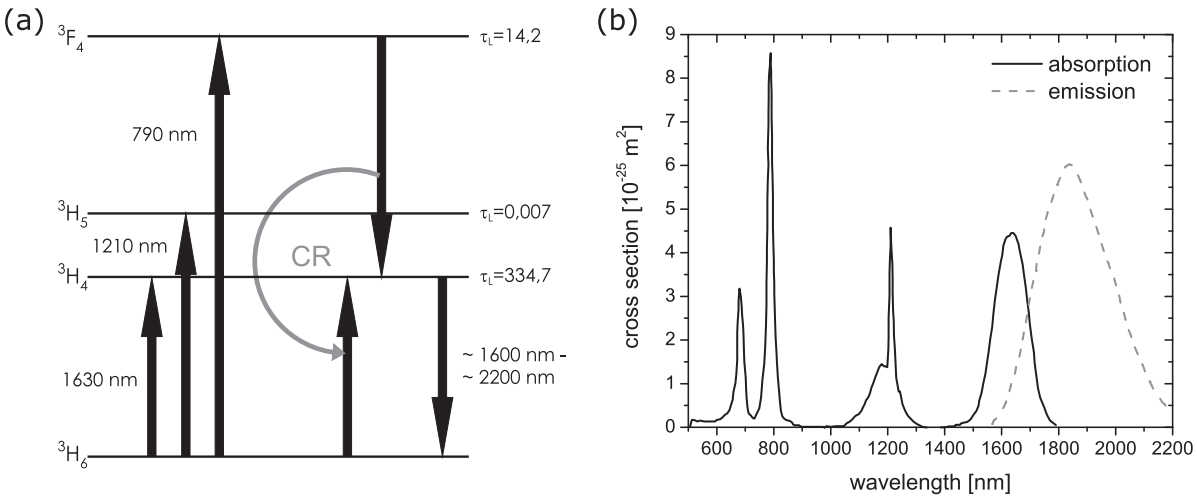

Figure 2.1: Spectroscopic properties of thulium doped silica fibers. (a): Simplified transitions scheme; (b): absorption (black solid curve) and emission cross section (grey dashed curve) [12].

10 W of output power at an emission wavelength of 790 nm are commercially available. In spite of the large Stokes-shift between pump and emission wavelength, thulium-doped fibers can be efficiently pumped at 790 nm due to a cross relaxation (CR) process, which is also indicated in Fig. 2.1 (a): If the thulium doping concentration is sufficiently high, the energy, which is released during the transition of an excited thulium ion from the $^3F_4$-level to the $^3H_4$-level, can be transferred to a nearby ion to excite the upper laser level. Due to this process, a quantum efficiency of 1.8 could be demonstrated with a thulium-doped germanate glass fiber and, consequently, the efficiency given by the quantum limit between pump and emission wavelength could be significantly exceeded [13].

However, the beam quality of these high power diode lasers is not sufficient for pumping directly into a core of a single-mode fiber. Therefore, 790 nm pump sources are typically used for a cladding pumping scheme, enabling output powers in the Watt regime.

The mostly used emission band of thulium-doped fibers extends from about 1.6 to above 2.2 µm, see Fig. 2.1. The corresponding amplification band typically ranges from around 1.85 to 2.05 µm [14, 15], where the amplification on the short wavelength side is limited by reabsorption and on the long wavelength side by the decreasing emission cross section. Accordingly, since saturation of the pump absorption is significantly higher,

core-pumping typically shifts the maximum gain to shorter wavelengths compared to cladding pumping schemes.

2.2 Pulse propagation in fibers

An ultrashort pulse, propagating in a transparent medium is influenced by several linear and nonlinear effects changing its shape and dimension in the temporal and frequency domain. In an isotropic medium, these effects can be considered via the refractive index, which then can be written as linear superposition [16]:

$$\tilde{n}(\omega, I) = n(\omega) + n_2 I \tag{2.1}$$

In this simplified expression, the linear refractive index $n(\omega)$ depends only on the frequency, while the nonlinear dependency, which is often called Kerr-effect, is implemented via the product of the nonlinear-index coefficient n_2 and the intensity I. In the following sections, several effects resulting from this dependency are introduced.

2.2.1 Chromatic dispersion

Due to the relation of pulse duration and spectral bandwidth, chromatic dispersion is a key phenomenon in the context of ultrashort pulses. It results from a frequency-dependent phase and group velocity and can mathematically be described via a Taylor expansion of the mode propagation constant β around a center frequency ω_0 [16]:

$$\beta(\omega) = n(\omega)\frac{\omega}{c} = \beta_0 + \beta_1(\omega - \omega_0) + \frac{1}{2}\beta_2(\omega - \omega_0)^2 + \cdots, \tag{2.2}$$

where $n(\omega)$ is the frequency-dependent refractive index, c is the speed of light and

$$\beta_m = \left(\frac{d^m\beta}{d\omega^m}\right)_{\omega=\omega_0} \qquad (m = 0, 1, 2, ...). \tag{2.3}$$

The parameters β_m correspond to the respective order dispersion terms, where the second order dispersion (SOD) term β_2 is referred to as group velocity dispersion (GVD) and

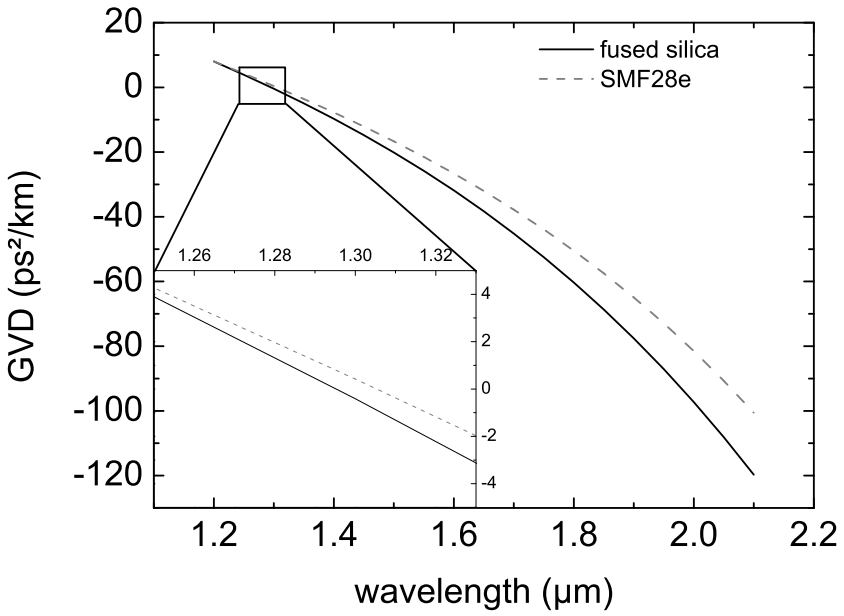

Figure 2.2: Dispersion of fused silica (black continuous curve) and SMF28e fiber (grey dashed curve).

$\beta_1 = 1/v_g$. The dispersion contribution $\beta_2 \cdot L$ of an optical element with the length L is denoted as group delay dispersion (GDD).

If an ultrashort pulse propagates in a dispersive medium its spectral components experience a temporal delay. Hence, an initially Fourier-limited pulse temporarily broadens, it becomes "chirped". While the spectral chirp only depends of the amount of accumulated phase, the corresponding temporal broadening scales with the spectral width. Therefore, the relevance of dispersion relates inversely proportional to the Fourier-limited pulse duration.

In an optical fiber, the dispersion consists of contributions by material and waveguide properties. Above a wavelength of about 1.27 µm, the dispersion of fused silica becomes anomalous, corresponding to a negative β_2 coefficient. In the thulium amplification window, the material dispersion is around -90 ps^2/km.

In contrast to material dispersion, the contribution of waveguide dispersion of standard step-index single-mode fibers is always normal. This is exemplary shown in Fig.2.2, where the dispersion curve of fused silica is compared to a standard SMF28e fiber. Consequently, waveguide dispersion shifts the point of zero dispersion towards longer

wavelengths. The amount of waveguide dispersion depends on the overlap between the fundamental mode and the fiber core and consequently is mainly determined by the core radius and the numerical aperture (NA).

2.2.2 Nonlinear effects

According to equation (2.1), the refractive index of fused silica does not only depend on the wavelength, but also changes with the intensity of a propagating electromagnetic wave. Although the nonlinear index coefficient n_2 of fused silica, which is the main constituent of standard optical fibers, is not very large compared to other materials, nonlinearity can have significant influence on a pulse propagating in an optical fiber due to the long interaction distances and high intensities. Various effects result from this nonlinearity.

Self-phase modulation

Besides chromatic dispersion, self-phase modulation (SPM) plays a key role in the formation of ultrashort pulses propagating in an optical fiber. SPM denotes a self-induced nonlinear phase shift, related to the nonlinear refractive index change, which is given by [16]:

$$\Phi_{NL}(T) = n_2 \cdot \frac{2\pi}{\lambda} \cdot L \cdot I(T) = n_2 \cdot \frac{2\pi}{\lambda} \cdot L \cdot \frac{P(T)}{A_{eff}} = \gamma \cdot L \cdot P(T) \tag{2.4}$$

where γ is the nonlinear coefficient, L the propagation distance, A_{eff} the effective mode-field area and $I(T)$ and $P(T)$ the intensity and power depending on the time T, respectively.

According to equation (2.4), the nonlinear phase shift, which is also often referred to as B-integral, goes along with a change of the instantaneous frequency of a propagating pulse. This change is proportional to the negative derivative of the temporal pulse shape, and therefore modifies the optical spectrum. While at the leading edge of the pulse, the instantaneous frequency decreases, it is increased at the trailing edge of the pulse. Consequently, with an initially unchirped or positively chirped pulse, additional

spectral components are generated via SPM and the pulse spectrum broadens. Contrary, a negative chirp causes annihilation of spectral components and thus a decrease of the spectral bandwidth.

Cross-phase modulation

cross-phase modulation (XPM) is an additional intensity-dependent shift of the optical phase, similar to SPM. In contrast to SPM, the change of the refractive index related to the phase shift by XPM is not induced by the electromagnetic wave itself, but by a second field with different wavelength, propagation direction or polarization. The combined nonlinear phase shift, the first field experiences, is then given by [16]:

$$\Phi_{NL} = \gamma \cdot L \cdot (P_1 + \alpha P_2). \tag{2.5}$$

In isotropic media, α becomes 2 for electromagnetic waves with the same polarization and 2/3 for fields with crossed polarization [16]. In context of an ultrashort pulse propagating in non-polarization-maintaining fibers, especially the latter case is relevant due to intrinsic or stress-induced birefringence. Even if the initial polarization is, for example, linear, it will become elliptically inside the fiber. The resulting polarization components affect each other during propagation and cause an intensity-dependent rotation of the polarization state.

Intrapulse Raman-scattering

Raman-scattering is a nonlinear effect, where photons are inelastically scattered by optical phonons. During this scattering process, parts of the photon energy are transferred to the phonon resulting in a frequency red-shift of the photon, which provides additional amplification in the lower frequency range with a maximum around 13.2 THz [16]. Consequently, if the optical spectrum of a pulse is sufficiently broad, scattered high frequency photons can cause amplification of low frequency components of the pulse spectrum resulting in a red-shift of the spectral centroid. This process is called intrapulse Raman scattering (IRS).

Self-steepening

Corresponding to equation (2.1), the refractive index and consequently the group velocity depends on the intensity of an electromagnetic field. Referring to a pulse propagating in a fiber, this induces an effect, which is called self-steepening: The center of a pulse, where the intensity is high, travels at a lower speed as the low intensity pulse wings. Hence, it becomes temporarily delayed causing a decreasing slope at the leading and an increasing slope at the trailing edge of the pulse. Due to SPM, the resulting asymmetry of the temporal pulse shape also leads to an asymmetric spectrum.

Modulation instability

Modulation instability (MI) denotes a further phenomenon that describes the breakup of a continuous wave (CW) or quasi-CW signal propagating in an anomalous dispersion fiber. Due to the interplay of the anomalous GVD and SPM, initially small fluctuations of the signal grow with the propagation in the fiber and finally lead into the breakup of the signal into a train of ultrashort pulses. This breakup is accompanied by the occurrence of sidebands in the optical spectrum. The maximum of the first sidebands is related to the fiber parameters and the signal Power P_0 via [16]:

$$\Omega_{max} = \pm\sqrt{\frac{2\gamma P_0}{|\beta_2|}} \tag{2.6}$$

MI are also relevant in the context of pulsed systems provided that the pulse duration is long compared to the modulation period [17].

2.2.3 Numerical modelling

The pulse propagation in optical fibers can be described in good approximation by the nonlinear Schrödinger equation (NLSE), which includes the effects of GVD and SPM [16]:

$$i\frac{\partial A}{\partial z} = \frac{\beta_2}{2}\frac{\partial^2 A}{\partial T^2} - \gamma|A|^2 A \tag{2.7}$$

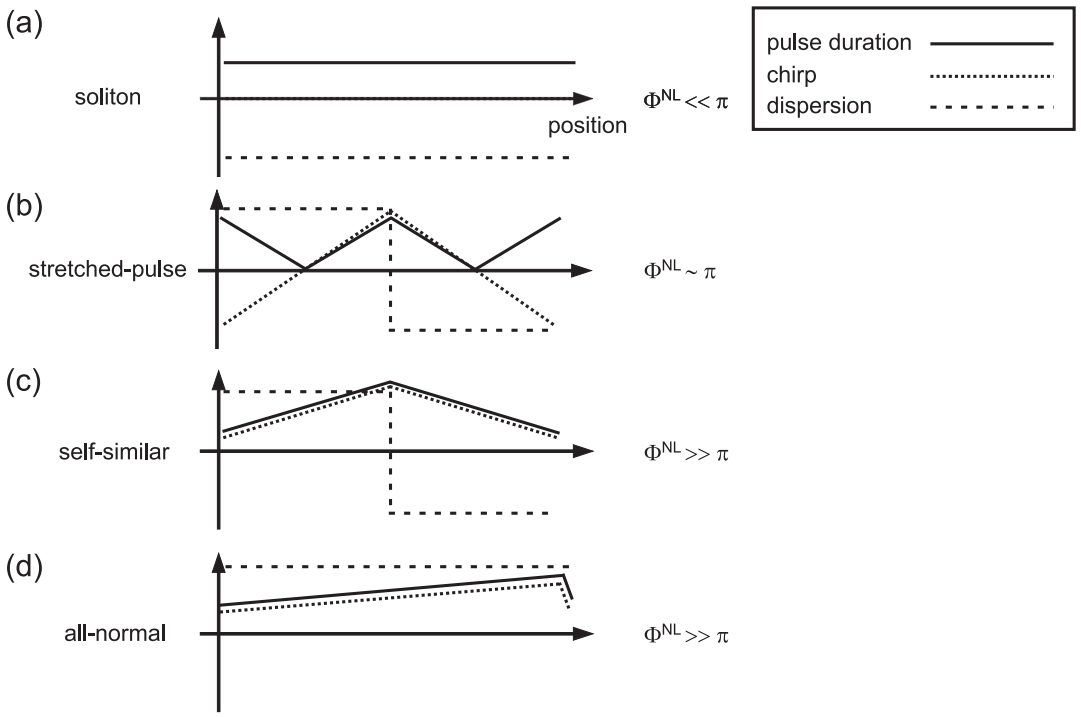

Figure 2.3: Schematic of the pulse regimes in ultrashort pulse fiber lasers [18].

Here, the envelope $A(z,t)$ is estimated to be slowly varying relative to the electromagnetic field itself and normalized such that $|A|^2 = P$. The propagation is considered in the retarded time frame, which is moving in z-direction at the group velocity v_g, related to the real time t via $T = t - z/v_g$ [16].

To implement further effects like gain and loss, higher order dispersion terms and other nonlinear parameters, the NLSE can be extended making it suitable for modelling the pulse propagation in a fiber oscillator. The extended NLSE can then be solved using the split-step Fourier transform method: Dispersive and nonlinear effects are alternately applied each for a short propagation distance, where a fast Fourier transform algorithm is used to switch between both domains. This process can successively be executed for the different fiber sections and components of the laser until a state is reached, which reproduces itself after one resonator round trip.

2.3 Pulse regimes in fiber lasers

As elaborated in section 2.2, the spectral and temporal shape of an ultra-short pulse are influenced by a number of effects during propagation along an optical fiber. Nevertheless, in a laser, the boundary condition has to be fulfilled that the electromagnetic field and hence the circulating pulse reproduces itself after one cavity round trip. As a result, different operation schemes have been developed, where these effects are balanced either locally or averaged over one cavity round trip. These can roughly be divided into four regimes, which are sketched in Fig 2.3 and will be introduced in the following.

2.3.1 Soliton

In case of anomalous fiber dispersion, the laser can be operated in the fundamental soliton regime. Here, the negative dispersive phase shift is locally balanced via the positive contribution by SPM (Fig 2.3 (a)). The temporal pulse shape is then described by a sech^2-function and propagates chirp-free and with constant duration, where the pulse energy E_P and duration τ are related via the "soliton area theorem" [16]:

$$E_P \cdot \tau = 2 \cdot \frac{|\beta_2|}{\gamma} \tag{2.8}$$

Soliton pulses are very stable with respect to perturbations. If the parameters of an input pulse do not exactly meet equation (2.8), it will evolve towards the corresponding pulse shape by exchanging energy with a copropagating background, which is denoted as dispersive wave. For this reason it is possible to generate solitons in fiber lasers, where such perturbations are repeatedly introduced due to gain and losses.
In case of periodic amplification, this dispersive wave becomes visible as side-peaks in the optical spectrum, which are referred to as Kelly-sidebands. The position of these sidebands is determined by the phase matching between the dispersive wave and the soliton spectrum and thus depends on the dispersion, the pulse duration and the amplification period [19].
However, the drawback of soliton lasers is that they are very limited in terms of pulse

energy and consequently duration. Soliton fiber lasers operating around 2 µm typically deliver pulses with a duration of around 1 ps and correspondingly several 100 pJ of energy [3, 5, 20]. Besides the limited maximum nonlinear phase shift accumulated during a resonator roundtrip a soliton can tolerate, the effect which mostly imposes the limitation of the pulse energy is related to the stabilizing mechanism. Increasing the pump power above a certain level does not lead to higher pulse energies, but mainly to an increase of the dispersive wave. If the pump energy is then further increased, the pulses finally break up. Therefore, the onset of Kelly-sidebands is a reliable indication that the pulse energy achieved its maximum value.

2.3.2 Stretched-pulse

To overcome the pulse energy limitation of the fundamental soliton regime, a dispersion management can be introduced by implementing segments with alternating dispersion into the cavity. With a cavity dispersion around zero, the laser can be operated in the stretched-pulse regime, which is depicted in Fig 2.3 (b). This regime is characterized by a 'breathing' dynamic of the pulse duration. The pulse chirp mainly linearly alternates with the dispersion changing its sign and consequently reaching a minimum duration in each dispersion segment. The exact position of the points of minimum duration shifts with the resonator GDD and the nonlinear influence [21].

As in stretched-pulse lasers the pulse is chirped during most of the propagation, it accumulates less nonlinear phase. In addition, this propagation scheme can tolerate a significantly higher nonlinear phase shift compared to fundamental solitons. Consequently, the pulse energy can be increased by about an order of magnitude compared to fundamental soliton fiber lasers [22].

Nevertheless, the pulse energy is still limited by the nonlinear influence around the points of minimum pulse duration. At this position, the pulse reaches the highest peak intensities and thus becomes mostly influenced by fiber nonlinearity. With excessive nonlinear phase, the pulse chirp can become nonmonotonic, which either leads to optical wave-breaking or soliton compression and thus to destabilization of the pulse propagation [23].

2.3.3 Positively chirped pulse

In the fundamental soliton and stretched-pulse operation, nonlinearity imposes a destabilizing mechanism and therefore needs to be reduced to achieve higher pulse energies. In contrast, in lasers with positively chirped pulse operation (PCP) schemes, it is taken advantage of that it can also contribute to the stabilization of ultrashort pulse propagation. The PCP-regime in fiber lasers is based on a publication by Anderson et al., in which the combination of gain, normal GVD and SPM was found to provide an asymptotic solution for a propagating pulse with a constant chirp and a parabolic temporal profile [23]. Due to GVD and SPM, positively chirped pulses propagating in a fiber with normal dispersion broaden temporarily as well as spectrally. Hence, for generation of positively chirped pulses in a laser, this broadening has to be reversed after each resonator roundtrip, which requires strong temporal or spectral filtering. The key feature enabling lasers with positively chirped pulse operation (PCP) schemes here is the linearisation of the chirp during the propagation [18]. PCP schemes can be manifoldly subdivided [24], however, for the most part this distinction is not relevant in the context of this work.

The first experimental realization of PCP in a fiber laser was the so called "similariton"-laser [2]. Similar to stretched-pulse lasers, the cavity contains segments with alternating dispersion. However, in this case the GDD of the anomalous fiber segment is only partly compensated and consequently the laser is operated with significant positive GDD. The resulting propagation scheme is depicted in fig 2.3 (c). The pulse chirp alternates mainly linearly with the fiber dispersion, but remains positive at every point inside the cavity and consequently reaches a minimum duration once at the beginning of the normal dispersion fiber section. The remaining spectral phase accumulated during each resonator roundtrip is balanced by SPM, while dissipative processes play only a secondary role for the pulse stabilization [25].

As stated before, due to the positive chirp, SPM leads to spectral broadening of the pulse. As the pulse is significantly chirped, this broadening is reversed simultaneously by temporal filtering at a saturable absorber. This also indicates a reversed concept,

sketched in Fig 2.3 (d), which is denoted as "all-normal" or "dissipative soliton". Here, the cavity consists only of fibers with positive GVD. Instead of segments with anomalous GVD, a spectral filter was implemented, which cuts back the optical spectrum and thus reverses the spectral as well as temporal broadening. The term "dissipative soliton" is attributed to the fact that in this operation regime spectral and temporal filtering plays a key role in the stabilization of the laser operation [18].

2.4 Ultrashort pulse generation in fiber lasers

Besides the cavity boundary condition, a further prerequisite to generate ultrashort pulses in a laser is that pulsed has to be preferred over CW operation [26]. This condition can be satisfied by a saturable absorber, which discriminates lower against higher intensities. For this purpose, a number of different absorber schemes are available, which are divided into 'real' and 'artificial' absorber mechanisms. In the following, two of them are introduced, which are relevant to the context of this work.

Semiconductor saturable absorbers

Semiconductor saturable absorbers are a typical representative of 'real' saturable absorbers. They are based on an interband transition in a semiconductor quantum well, typically InGaAs or GaAs. Their spectral absorption properties are determined by the bandgap between the valence and the conduction band. By absorption of photons, electrons are excited from the valence band to the conduction band until this is sufficiently occupied and the absorption reduces.

The absorption losses of a semiconductor saturable absorber can be adapted over a wide parameter range. In fiber lasers, typical modulation depths are around 10 to 20 %. The second relevant absorber parameter, the saturation fluence, is typically around several $\mu J/cm^2$ so that the spot size required to saturate the absorption with typical fiber laser pulse parameters matches the order of magnitude of the fiber mode-field diameter.

While the absorption is nearly instantaneous, the relaxation time of semiconductor sat-

urable absorbers is typically in the order of several hundred femtoseconds to several tens of picoseconds [27]. Thus, for shorter pulses, only the leading edge of an incoming pulse is influenced by the absorber, while the trailing edge remains nearly unaffected. Semiconductor saturable absorbers are therefore not suitable for the use in lasers with very short pulse durations, in which the pulse shaping by the saturable absorber is crucial for the stability of the operation regime.

Semiconductor saturable absorbers are often used in combination with a reflective Bragg-structure and then are denoted as semiconductor saturable absorber mirror (SeSAM) or saturable Bragg reflector (SBR). The SBR can be implemented as end mirror in a linear cavity configuration or via a σ-arm in a ring resonator. To avoid an internal cavity, which would limit the reflection bandwidth and introduce additional dispersion, the Bragg-structure has usually an anti-resonant design [27]. Nevertheless the bandwidth of SBRs is typically limited by the reflection bandwidth of the Bragg-structure.

Nonlinear polarization evolution

'Artificial' saturable absorbers are often based on the optical Kerr-effect. Among others, in optical fibers nonlinear polarization evolution (NPE) can be utilized to introduce an intensity-dependent loss mechanism. The functional principle is sketched in Fig. 2.4: Due to XPM and SPM, an initially elliptically polarized pulse experiences a nonlinear rotation of its polarization during propagation. Consequently, after propagation through the fiber, the polarization of the pulse maximum and the wings differs. Via a polarization-selective element, this rotation can be transferred into an intensity-dependent loss and thus provides saturable absorption.

In contrast to most 'real' saturable absorption mechanisms, for which the relaxation time typically cannot be neglected, the transmission of an absorber based on the Kerr-effect varies quasi instantaneous with the pulse intensity [28]. Therefore, they are suitable for the generation of pulses with several ten femtoseconds duration.

However, in terms of self-starting and stability, NPE has several drawbacks compared to real saturable absorber schemes. With real saturable absorbers, CW operation is efficiently suppressed and consequently the mode-locking threshold mostly corresponds

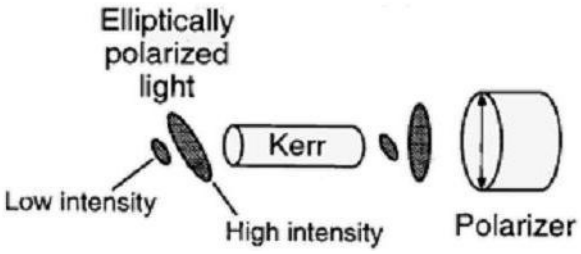

Figure 2.4: Schematic of saturable absorption based on nonlinear polarization evolution [21].

to the pump power required for stable single pulse operation. With artificial absorbers, the starting pulse has to evolve from arbitrary fluctuations during CW operation [28]. Therefore, typically the pump power needs to be enhanced in order to initiate mode-locking and is reduced afterwards for stable single-pulse operation. Furthermore, lasers mode-locked by real saturable absorbers are typically less sensitive to parameters like the waveplates setting and thus can be operated in a wider parameter region.

3 Stretched-pulse laser

In the previous chapter, the various cavity-internal pulse propagation schemes have been introduced. In the 2 µm spectral region, silica fibers typically provide anomalous dispersion and, therefore, thulium-doped fiber lasers can easily be operated in the fundamental soliton regime. However, this regime is very limited in terms of pulse energy and duration. To overcome this limitation, the laser can be operated in the stretched-pulse regime, which requires the implementation of normal GDD for dispersion compensation. Therefore, in this chapter, stretched-pulse operation of a thulium-doped fiber laser is investigated and described numerically and experimentally. Normal GDD is provided by a grating arrangement in combination with a telescope. The experimental and numerical setups are introduced in section 3.1 and 3.2, respectively. In section 3.3, variation of the pulse parameter with cavity dispersion and pump power is presented. The cavity dispersion was continuously varied between -0.044 ps^2 and +0.0495 ps^2. Dependence of the output parameters on the pump power at positive and negative cavity dispersion was examined for -0.0275 ps^2 and +0.0385 ps^2.

3.1 Experimental setup

The experimental setup is schematically shown in Fig 3.1. The laser was arranged in a ring resonator configuration with a repetition rate of 37.6 MHz. The active fiber was a thulium-doped double-clad fiber with a length of 2.5 m, a signal core diameter of 25 µm (0.1 NA) and a pump cladding diameter of 250 µm (0.46 NA). The fiber absorption at the pump wavelength of 793 nm was 5 dB/m as given by the fiber manufacturer. As pump source, a fiber coupled diode laser with a maximum output power of 25 W at 793 nm was used, which was free-space coupled into the fiber section via a dichroic

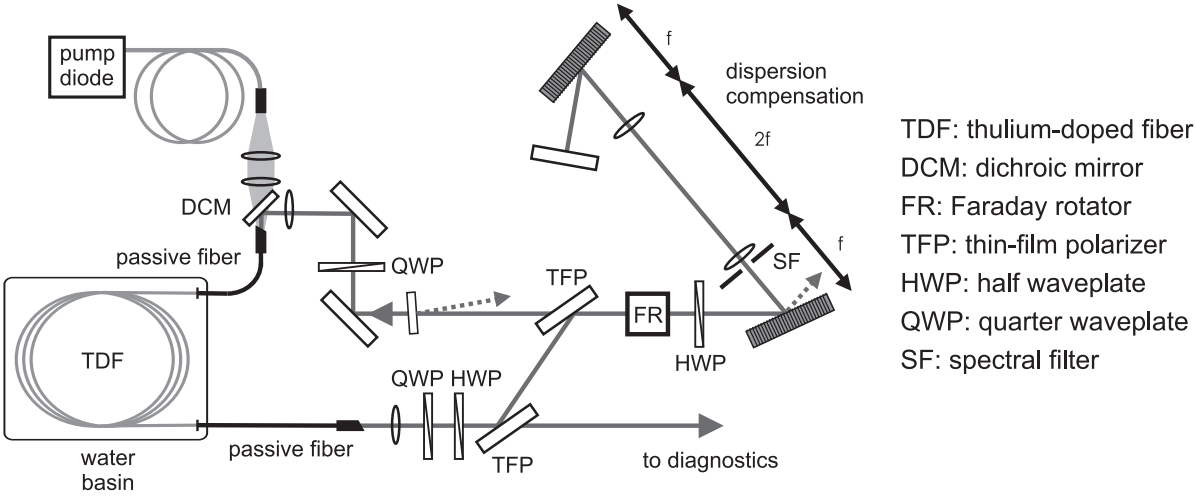

Figure 3.1: Schematic of the experimental setup

mirror (DCM). Two passive fiber pigtails with a length of 0.5 m at the pump end and 1 m at the outcoupling end were added to enable temperature stabilization in a water basin over the entire length of the active fiber. The core and cladding diameter as well as the cladding NA of the passive pigtails were identical to the active fiber while the core NA of 0.056 was lower. Consequently, the active fiber supported propagation of at least two transversal modes, while in the fiber pigtails only the fundamental mode was guided. Both ends of the fiber section were angle cleaved to avoid parasitic effects caused by Fresnel reflections, which can inhibit mode-locked operation [29]. Due to the large core diameter, the fiber GVD was dominated by material dispersion and thus was estimated to be about -0.09 ps^2/m resulting in an overall GDD of the fiber section of -0.36 ps^2 at 1980 nm.

For compensation of the fiber GDD a grating arrangement based on two anti-parallel reflection gratings and a telescope in 4-f-configuration was inserted into the cavity. The telescope permits negative effective distances between the gratings and consequently provides positive GDD [30]. With this setup, the cavity dispersion could easily be adjusted by varying the grating distance. To stabilize mode-locked operation, a spectral filter consisting of two razor blades with variable gap was inserted into the dispersion compensation section.

Mode-locking was achieved via nonlinear polarization evolution in the fiber. As polar-

ization selective element a thin-film polarizer (TFP) following the fiber section was used, which also acted as variable output coupler. The polarization dependent diffraction efficiency of the gratings in combination with the Faraday rotator (FR) and the preceding TFP ensured the unidirectional operation of the laser, which facilitates self-starting of mode-locked operation [29]. The reflected light from the input grating of the dispersion compensation section was used as a monitor port to gain information about the cavity internal spectrum and power. A further monitor port was inserted before the fiber section via a plane substrate with a one-sided anti-reflective coating.
For the external pulse recompression, a grating arrangement similar to the one applied for the cavity internal dispersion compensation was used.

3.2 Numerical model

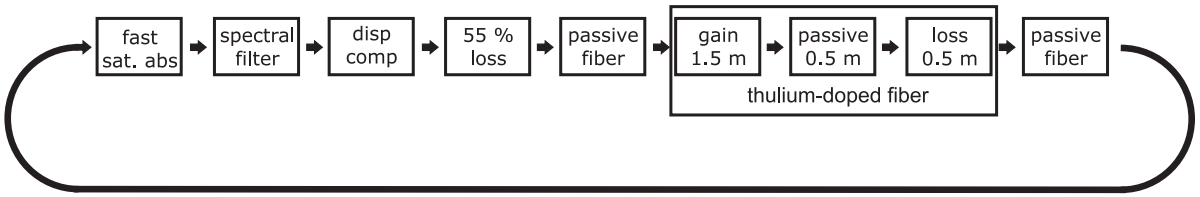

Figure 3.2: Schematic of the numerical simulation model.

Numerical simulations of the cavity-internal pulse propagation were performed with the commercial software Fiberdesk solving the extended nonlinear Schrödinger equation by the split-step Fourier method [31]. Linear effects included were saturable gain, loss and GDD; as nonlinear effects SPM, Raman response and self steepening were taken into account. Higher order dispersion has been neglected as no reliable data were available. The simulations started from quantum noise and were executed in loop until a steady state was reached. The detailed model (Fig. 3.2) comprised nine elements: The free space section (FS) consisted of a fast saturable absorber, a spectral filter and the dispersion compensation section, followed by a lumped loss of 55 %, which represented the overall linear loss of the dispersion compensation section. The reflectivity of the saturable absorber, which corresponds to the transmission of the polarization selective element for

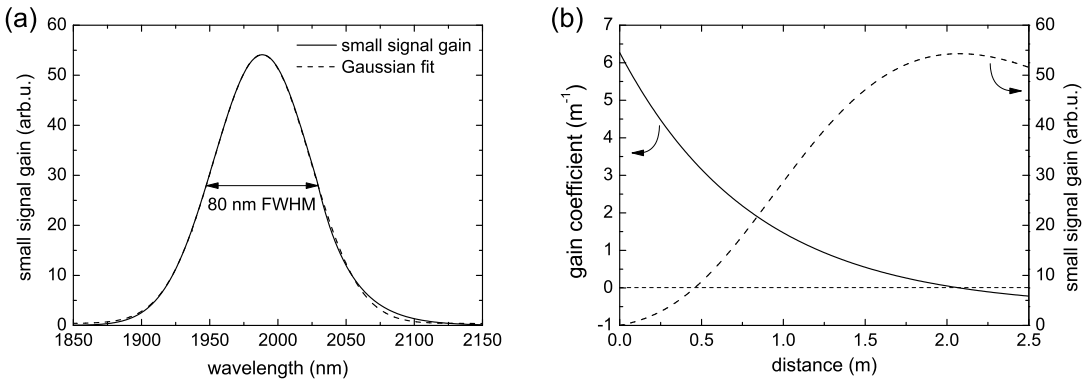

Figure 3.3: Simulations of the fiber amplification for 6.5 W of launched pump power: (a) spectral distribution (continuous curve) with Gaussian fit (dashed curve); (b) gain coefficient (continuous curve) and integrated small signal gain (dashed curve) versus longitudinal propagation at 1980 nm.

the NPE, is given by $R = R_0 + \Delta R - \frac{\Delta R}{1 - \frac{|A(T)|^2}{P_A}}$. Here R_0 is the linear reflectivity, ΔR the saturable reflection coefficient, $|A|^2$ the instantaneous power, T the time in the retarded time frame and P_A the absorber saturation power coefficient.

The fiber section consisted of three main segments, in which the active fiber was subdivided into three elements. This subdivision was implemented, since with the gain being homogeneously distributed along the complete active fiber the experimentally observed output characteristics could not be reproduced. The spectral and longitudinal gain distributions were estimated using a model by Pfeiffer and Bülow [32] and are displayed in Fig. 3.3. This model was selected since all parameters, which were necessary for the calculation of the fiber gain, could either be easily measured or were given by the fiber manufacturer. However, the model represents a relatively simple 2-level-approach, in which neither upconversion and cross relaxation nor saturation effects are included. Nevertheless, as for the implemented fibers most of these effects are assumed to have only minor influence, it was regarded to be sufficiently accurate for an approximate modelling of the fiber amplification.

The spectral gain function was approximated by a Gaussian shape with a full width at half maximum (FWHM) of 80 nm at a central wavelength of 1980 nm (cf. Fig 3.3 (a)), the saturation energy was set to 1 nJ. Corresponding to the gain distribution depicted in Fig. 3.3 (b), the amplification was restricted to the first part with a length of 1.5 m,

while the following elements, each with a length of 0.5 m, were estimated to be passive and introduce a minor exponential reabsorption loss ($\alpha_L = -0.1\,\mathrm{m}^{-1}$), respectively.
Referring to Marcuse [33], the mode field diameters of the active and passive fiber were estimated to be 22 µm and 28 µm, respectively. The nonlinearity parameter was set to $n_2 = 3.2 \times 10^{-20}\,\mathrm{m}^2\,\mathrm{W}^{-1}$.
The simulations were started from quantum noise and executed in loop until a steady state was achieved with the pulse reproducing itself after each resonator roundtrip. For subsequent pulse compression, according to the experiments, dispersion corresponding to a grating arrangement was applied.

3.3 Experimental and numerical results

With appropriate setting of the waveplates position and the spectral filter, mode-locked operation was self starting at about 10 to 12 W of launched pump power, resulting in multiple pulse operation. The number of circulating pulses could be decreased by reducing the pump power until single pulse operation with a CW background was reached. The CW background could be suppressed by further reduction of pump power to about 6.6 W, resulting in clean, stable single pulse operation.
With increasing positive cavity dispersion, the laser showed a tendency to q-switched mode-locking at low pump powers, which was revealed by a low-frequency modulation of the pulse train and sidebands in the radio-frequency (RF) spectrum. Q-switching could be eliminated after start of mode-locked operation by adjusting the spectral filter to reduce the intracavity losses. Thus, for larger positive cavity dispersion stable CW mode-locking was not completely self-starting, but nevertheless could still be achieved easily.

3.3.1 Dispersion variation

Starting with positive dispersion of $+0.0495\,\mathrm{ps}^2$, the cavity dispersion was reduced gradually to $-0.0440\,\mathrm{ps}^2$ by adaptation of the grating distance while maintaining the waveplates and filter position and only adjusting the pump power for maximum single pulse

output power at each step. The filter transmission with a FWHM of 20.5 nm was estimated from measurements of the amplified spontaneous emission of the weakly pumped active fiber with and without blocking the backcoupling path. The experimental cavity dispersion values were calibrated according to the dispersion variation measurement assuming that the shortest pulse duration and maximum spectral bandwidth corresponds to the smallest cavity dispersion value.

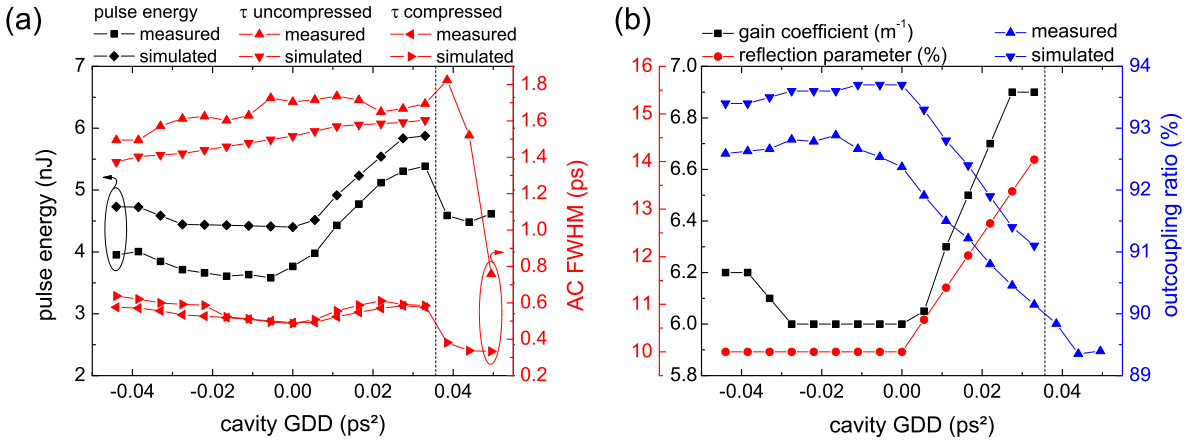

Figure 3.4: (a) Energy and AC FWHM of the measured/simulated pulses before and after compression versus cavity GDD; (b) gain and reflection coefficient and output coupling ratio in simulation and experiment.

Fig. 3.4 (a) shows the very good qualitative and quantitative agreement between experiment and numerical simulations in terms of pulse energy and AC FWHM before and after compression. For a cavity dispersion between -0.044 ps^2 and +0.035 ps^2 the resulting pulse energy and shortest pulse duration were in qualitatively good agreement with theoretical predictions as well as with previously reported experimental results [34, 35]. Both of them reveal a minimum at about zero dispersion and increase with positive as well as negative dispersion. The uncompressed pulse duration increased almost linearly over most of the dispersion range. As collinear autocorrelations were measured, the AC FWHM was estimated by applying a low pass filter onto the interferometric AC trace. The pulse energy increased only slightly with negative dispersion, but considerably with positive dispersion. A maximum pulse energy of 5.4 nJ was achieved at 0.0385 ps^2 of cavity dispersion. The internal and the externally measured pulse energy evolve in the

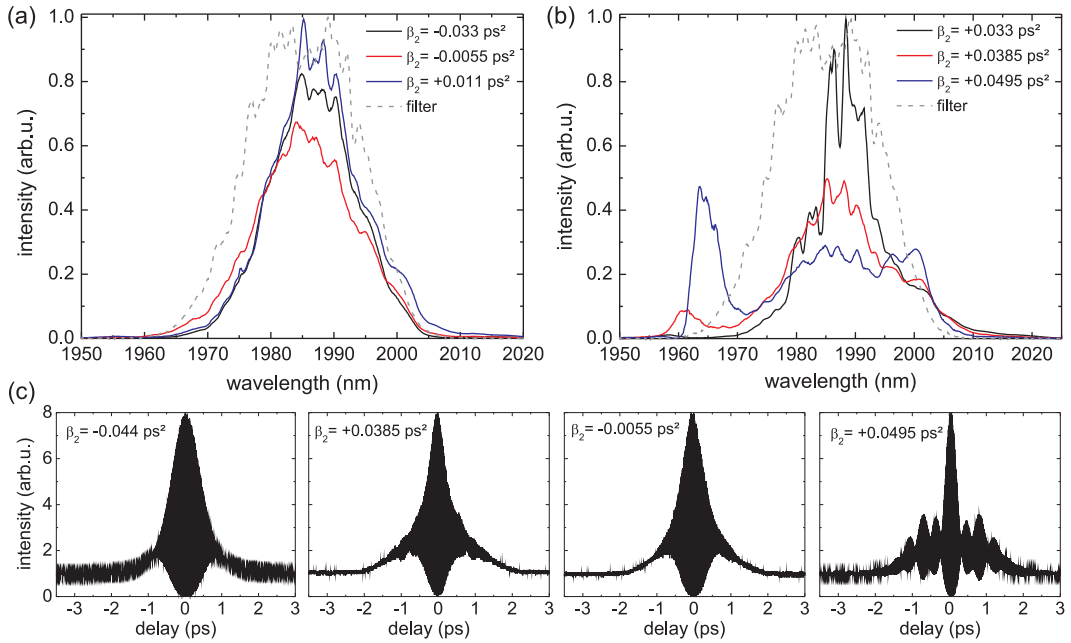

Figure 3.5: (a) Spectra with negative and nearly zero cavity dispersion, (b) spectra with positive cavity dispersion, each normalized regarding pulse energy and (c) corresponding autocorrelation traces.

same way, which is revealed by power measurements at the output and the monitor port and is in agreement with the simulations.

Fig. 3.4 (b) shows the gain and the reflection parameter ΔR of the saturable absorber from the simulation as well as the resulting outcoupling ratio in the simulation and the experiment versus the cavity dispersion. Comparable to the experimental condition, the gain and the saturable absorption coefficient were the only simulation parameters that were adapted for the respective dispersion compensation to match the experimentally observed characteristics. The remaining parameters of the saturable absorber (SAbs) were set to $R_0 = 1\,\%$ and $P_A = 2.5\,\mathrm{kW}$. Concerning the outcoupling ratio it must be taken into account that the intracavity power was evaluated from power measurements with a thermal sensor at the monitor port at sub mW power level. Therefore, the absolute values are not to be regarded as overaccurate. Nevertheless, the measurement should reflect the actual development qualitatively well.

In the negative cavity dispersion and slightly positive cavity dispersion regime, the shape

of the spectrum and AC trace remained nearly constant, while at higher positive cavity dispersion values significant changes could be observed. This is shown in Fig. 3.5 by means of selected spectra and AC traces. The modulations of the spectra and of the spectral filter originate from a wavelength-dependent transmission of the splices between the doped fiber and the passive pigtails, which could be verified by spectral measurements with and without the fiber pigtails.

Above $+0.0385\,\mathrm{ps}^2$ of cavity dispersion the spectrum broadened significantly and a side-peak developed around 1965 nm resulting in shorter Fourier-limited pulse duration. Simultaneously, the pulse energy decreased and the AC trace revealed a pedestal and sidelobes, which also remained, when the pulse was dechirped externally. For this dispersion region, the characteristics of the experimentally observed pulses could not be reproduced by the numerical simulations.

The deformation of the spectral shape and the increasing divergence of the experimentally observed characteristics from the simulations can be attributed to polarization effects like polarization mode dispersion (PMD) and particularly XPM. A number of arguments supports this explanation to be the most reasonable. As polarization effects are not included in the simulation software, this might explain deviations of simulation and experiment, especially in terms of the spectral asymmetry. Also higher order dispersion terms might cause spectral asymmetries. Nevertheless, the simulations offer good insight into the evolution of the pulse propagating inside the cavity.

The strongest indication for an increasing impact of XPM with positive dispersion is the decrease of the outcoupling ratio with increasing cavity dispersion. As the polarization at the beginning of the fiber section was kept constant during the whole experiment, varying nonlinear polarization rotation caused variation of the outcoupling ratio. The lower outcoupling ratio therefore is a result of higher saturation of the absorber owing to stronger nonlinear polarization rotation, which is induced by XPM. This stronger polarization rotation required an increase of the saturable reflection parameter to match simulation and experiment (see Fig. 3.4).

Regarding the evolution of pulse energy and duration as well as outcoupling ratio versus

cavity dispersion the pulse energy is estimated to be limited by nonlinear chirp contributions. Similar to optical wave-breaking with positive fiber GDD, excessive nonlinear phase contributions at negative GDD can cause a non-monotonic pulse chirp leading to a pulse breakup [36]. The other possible limiting effect, an overdriving of the saturable absorber mechanism, can be ruled out, since it would be inconsistent with the decrease of outcoupling ratio with increasing accumulated nonlinearity over most of the investigated range. Merely at major positive cavity dispersion, overdriving of the saturable absorber mechanism might be the limiting effect as indicated by the pulse energy, minimum duration as well as the outcoupling ratio remaining nearly constant.

3.3.2 Negative cavity dispersion

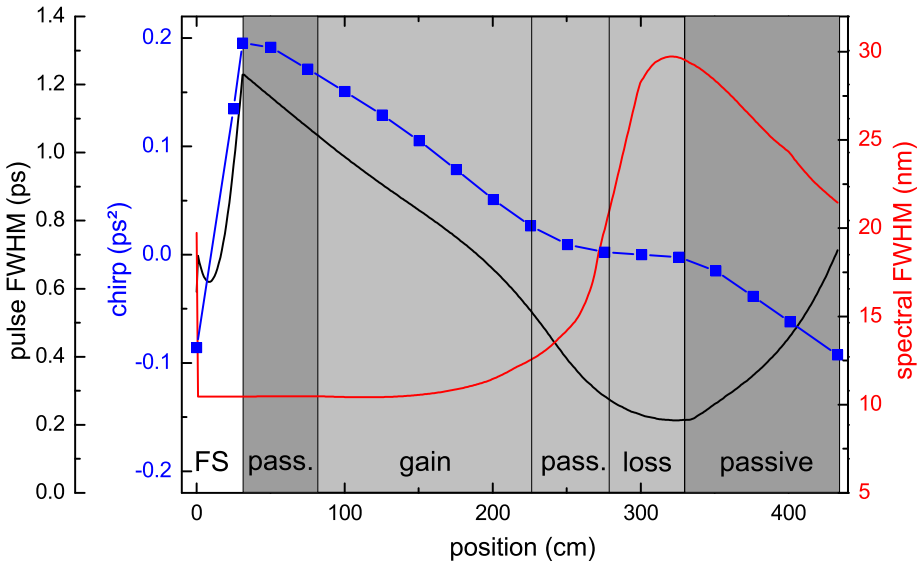

Figure 3.6: Simulated pulse FWHM, chirp and spectral FWHM versus propagation.

In Fig. 3.6, the spectral and temporal evolution as well as the chirp versus propagation distance of the simulated pulse for a single cavity roundtrip at a cavity dispersion of -0.0275 ps^2 is displayed. To match the experimentally observed parameters, the saturable absorber parameters for this configuration were set to $R_0 = 1\,\%$, $\Delta R = 8\,\%$ and $P_A = 2.5\,\mathrm{kW}$ and the gain was set to $g = 6.15\,\mathrm{m}^{-1}$. The transmission of the spectral filter with a FWHM of 15.2 nm at a central wavelength of about 1986 nm was estimated by

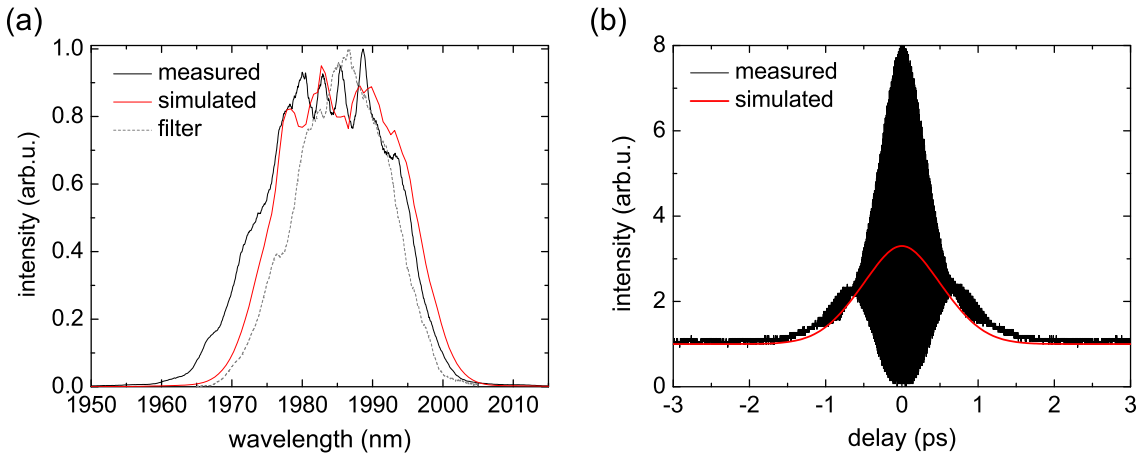

Figure 3.7: (a) Measured and simulated spectrum and (b) AC trace after the fiber section.

spectral measurements before and after the dispersion compensation section.

The evolution of pulse parameters confirms the stretched-pulse operation of the laser and reveals the influence of fiber nonlinearity on the propagating pulse. While the chirp evolution is mainly linear on the first 2 m and the last about 0.8 m of propagation inside the fiber section, it shows a plateau around 3 m, where the sign of the chirp changes. This plateau is attributed to the influence of the fiber nonlinearity on the chirp, which is also revealed by the increase of the spectral half-width from about 10 to 30 nm. The flattening is a further indication that the pulse energy is limited by soliton compression, since with higher pulse energy the nonlinear influence on the pulse chirp would become predominant resulting in a non-monotonic chirp evolution and consequently in pulse break-up [36]. Furthermore, the point of maximum spectral half-width and consequently of minimum pulse duration is shifted about 20 cm compared to the point of chirp sign change, which also reveals the high nonlinear influence, since for a linear propagation, this points would have to be expected at the same position.

Fig. 3.7 (a) and (b) show the very good spectral and temporal agreement of simulation and experimentally observed output pulse parameters, respectively. The simulated pulse energy of 4.2 nJ was slightly higher than the measured energy of 3.2 nJ. The simulated pulse duration at the end of the fiber section was about 700 fs. The pulses could exter-

nally be dechirped to 277 fs duration, which was 5 % above Fourier-limit.
Both in experiment and simulation, the spectral width at the end of the fiber section slightly increased about 1 nm, when the pump power and accordingly the gain parameter was reduced. This was caused by the pulse duration minimum shifting several centimeter towards the end of the fiber section resulting in reduced reconversion of spectral components. The shape of the spectrum and the AC trace remained basically unchanged.

3.3.3 Positive cavity dispersion

In the negative dispersion region, the pump power could only slightly be varied while maintaining stable laser operation and hence, the output pulse parameters were mainly determined by the cavity dispersion. Contrary, in the positive cavity dispersion regime, the output pulse characteristics significantly depended on the pump power. This corresponds to the results reported on in Ref. [35], in which for a fixed cavity dispersion in the negative dispersion regime only slight variations of the pulse energy could be observed while with positive cavity GDD the pulse energy could be varied by about a factor two. In Fig. 3.8, pulse parameters with varying pump power at $+0.0385\,\mathrm{ps}^2$ cavity dispersion are displayed. The spectrum was centered around 1985 nm with a side peak at around 1965 nm. With decreasing pump power the side peak increased and shifted towards longer wavelengths (Fig. 3.8 (a)), accompanied by a pedestal and side lobes occurring in the AC trace (Fig. 3.8 (c)). The pulse energy varied almost linearly with the pump power, while the Fourier-limited and compressed pulse duration remained nearly unchanged for low pump powers and slightly increased with higher pump power (Fig. 3.8 (b)). The dispersion of the external compression unit was kept constant during variation of pump power; therefore a shift of the minimum pulse duration position inside the resonator resulted in slight mismatch of pulse chirp and external dispersion compensation. The insets in Fig. 3.8 (c) show the AC traces after compression. The minimum pulse duration of 216 fs was achieved at 7.09 W of launched pump power.
The evolution of the spectral shape and the AC trace suggest that according to the negative dispersion regime increasing the pump power causes the position of minimum

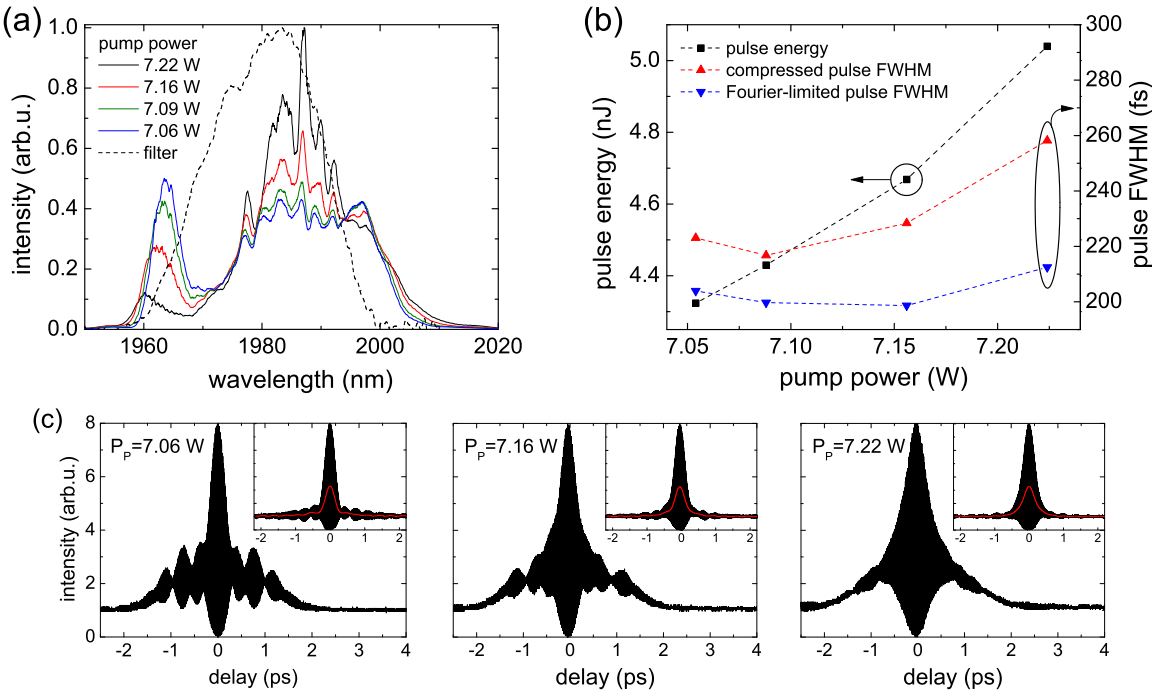

Figure 3.8: (a) Spectrum, (b) pulse energy and duration and (c) AC traces with varying pump power at $+0.0385\,\mathrm{ps}^2$ cavity dispersion. Insets: AC traces of the compressed pulses.

pulse duration shifting towards the pump end of the fiber. This is mainly indicated by the position of the spectral side peak indicating that a higher pulse energy corresponded to generation of a broader spectrum. However, owing to the shift of the pulse minimum position, most of the generated spectral components were reconverted resulting in a narrower spectrum at the end of the fiber.

3.4 Conclusion

In this chapter, the output characteristics of a spectrally filtered, stretched-pulse fiber laser were investigated by numerical simulations and experiments. Cavity dispersion was continuously varied between -0.0440 ps^2 and $+0.0495\,\mathrm{ps}^2$. The largest pulse energy could be achieved with normal cavity dispersion while still very short pulse durations could be maintained. A minimum pulse duration of 216 fs and a maximum energy of 5.4 nJ was achieved.

The variation of the output pulse parameters as a function of pump power was exemplary examined for -0.0275 ps^2 and +0.0385 ps^2 of cavity dispersion. While for anomalous cavity dispersion, the pump power could only slightly be varied and no significant changes in the output parameters were observed, at normal cavity dispersion the output characteristics strongly depended on the pump power. The variation of the output pulse characteristics could be attributed to a shift of the position of minimum pulse duration inside the resonator.

The experimental results agreed well with theoretical predictions [34] as well as previously reported results in the 1.5 µm spectral region [35] and could be reproduced very well by numerical simulations for a wide dispersion range. Deviations of experimental and numerical results were attributed to polarization effects, which were not included in the applied numerical software. The pulse energy was estimated to be limited by the onset of a nonlinear chirp.

4 Pulse amplification

As mentioned before, ultra-short pulse fiber lasers are always limited in pulse energy due to the fiber nonlinearity. If larger pulse energies are desired, the pulse energy can be increased by subsequent amplification stages. The advantages of a fiber based amplifier compared to solid-state setups are similar to lasers. Due to the higher average powers, especially the advantage of simple heat management becomes more relevant. However, higher intensities resulting from larger pulse energies are of course accompanied by increasing nonlinear effects. Different approaches take account of this fact.

The fiber nonlinearity can for example be used to increase the spectral bandwidth. If the pulse is positively chirped, the accumulated nonlinear phase results in the generation of additional spectral components leading to shorter Fourier-limited pulse durations. This has been utilized by Imeshev and Fermann [11]: Pulses with a nearly Fourier-limited duration of 150 fs at a center wavelength of 1980 nm and 0.6 nJ pulse energy were positively prechirped before launching them into the amplification fiber with anomalous dispersion. With this concept, pulse shortening to 108 fs duration and a pulse energy of 31 nJ could be achieved, limited by the available pump power.

If the spectral width of the seed pulse and the amplification is sufficiently broad, a Raman-soliton can be generated during the amplification process. This has been demonstrated by Kivistö et al. using Tm-Ho-doped fibers, which expands the amplification bandwidth above 2 µm wavelength. By amplifying pulses with 0.4 nJ energy and 750 fs duration at a center wavelength of 1.97 µm, a tunable output ranging from 1.97 µm to 2.05 µm and pulse shortening down to 150 fs with a maximum output pulse energy of 4 nJ could be achieved [5].

However, as pulses with excessive nonlinear phase break up, the concept of nonlinear spectral broadening inherently limits the maximum pulse energy. To overcome this issue,

the pulse peak intensity needs to be reduced. This can be achieved by increasing the mode-field diameter inside the fiber by extending the core diameter and reducing the NA. However, this concept is also limited, since the NA cannot be made indefinitely small for manufacturing reasons and consequently the number of transversal modes would increase with the core diameter.

Alternatively, for ultra-short pulses the peak intensities can be reduced by dispersive stretching. This concept is known as chirped-pulse amplification (CPA) and was first demonstrated by Strickland and Mourou [37], but had not been adapted to thulium-doped systems yet. In a CPA scheme, the pulse becomes dispersively chirped before and compressed after amplification. Thus, if the pulses are sufficiently stretched, a mainly linear amplification with negligible nonlinear influence can be achieved even at very large pulse energies.

In this work, the amplification with positive prechirping as well as CPA has been investigated. Amplification with prechirped pulses will be presented in section 4.1. The results with a CPA will be presented in section 4.2.

4.1 Amplification with positively prechirped pulses

As described above, the fiber nonlinearity can be utilized to achieve nonlinear shortening of the pulse duration by generation of additional spectral components. If the initial positive pulse chirp and the anomalous GDD of the amplifier fiber section are properly matched, the pulse reaches minimum duration at the end of the amplifier fiber section, where the pulse energy is maximal and consequently maximal spectral broadening and pulse shortening is achieved. Furthermore, no subsequent dispersion compensation is necessary.

4.1.1 Experimental setup

The amplifier setup is sketched in Fig. 4.1. It consisted of the seed oscillator, followed by a dispersive delay line (DDL) and an optical isolator to prevent back reflections, which could destabilize the oscillator. The following amplification fiber was the same

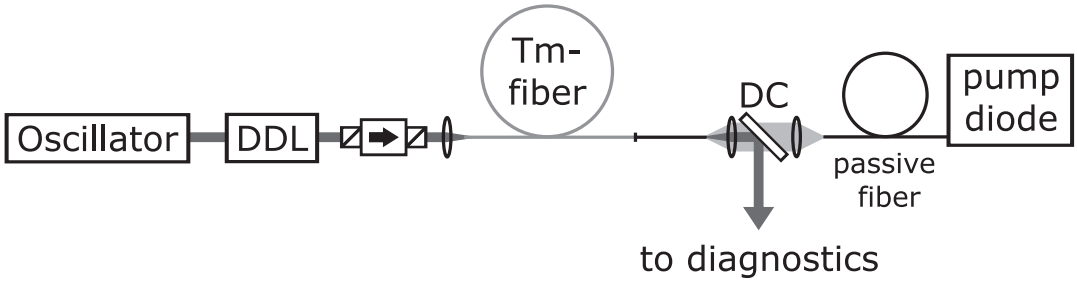

Figure 4.1: (a) Schematic of the experimental setup; DDL: dispersive delay line, DC: dichroic mirror.

type of fiber, which was used in the oscillator setup. It was a thulium-doped, double-clad large-mode area (LMA) fiber. The signal core diameter was 25 µm with a NA of 0.1; the pump cladding diameter and NA were 250 µm and 0.46, respectively. Based on numerical calculations with a model developed by Pfeiffer and Buelow [32], which was introduced in section 3.2, a length of 2.8 m of the active fiber was chosen to achieve the highest gain at the seed wavelength of 1980 nm by avoiding reabsorption losses due to weakly pumped fiber regions. For maximum amplification efficiency, the active fiber was free-space cladding-pumped in reverse direction by a 25 W fiber-coupled pump diode at 793 nm, absorbing 96 % of the launched pump power. The coupling efficiency of the pump light into the fiber section was about 80 % due to the relatively large focal distances and the resulting abberations of the standard plano-confex lenses. Pump and signal propagation were seperated by a dichroic mirror between the lenses. To avoid pointing instabilities due to thermally induced movement of the pump end of the fiber section, a 50 cm passive fiber pigtail with the same dimensions and NA was added to the amplifier fiber at the pump end.

As seed source, the laser described in chapter 3 was used. The DDL was a grating arrangement, similar to the one inside the laser cavity to compensate for the negative pulse chirp of the seed laser and the anomalous amplifier dispersion. The shortest pulse duration at the end of the amplification fiber could be achieved with a dispersion of about 0.36 ps^2 GDD at 1980 nm.

4.1.2 Amplification results

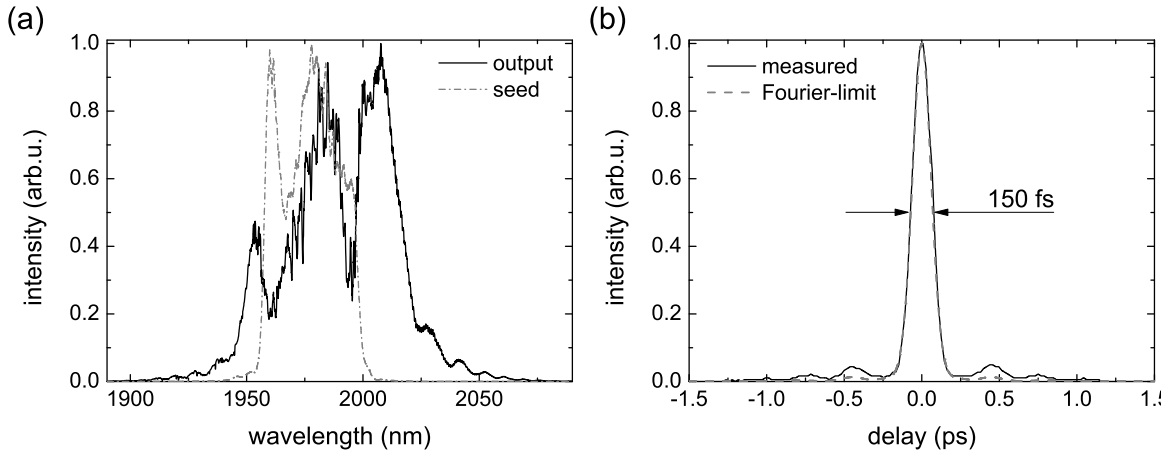

Figure 4.2: (a) Optical seed (grey dashed-dotted curve) and amplifier output spectrum (black continuous curve); (b) AC trace measured at the amplifier output (black continuous curve) and Fourier-limited (grey dashed curve).

In Fig. 4.2, the amplifier's spectral and temporal output at 6.8 W of launched pump power is displayed. Fig. 4.2 (a) shows the optical spectrum before (grey curve) and after (black curve) amplification. The spectral shape of the amplified pulses is primarily given by the seed spectrum, but significantly broadened. The root mean square (RMS)-width doubled from 12 to 24 nm. Especially in the center of the spectrum, where the output and the seed spectrum overlap, modulations with a fringe distance of about 1.2 nm can be found. As will be shown in section 4.2, these can be attributed to interference between the fundamental and the higher LP11 transversal mode. The slightly different effective refractive index of these modes leads to a temporal delay, which becomes apparent in the spectral modulations.

Fig. 4.2 (b) reveals very good agreement of the measured (black continuous curve) and the Fourier-limited (grey dashed curve) AC trace. Accordingly, the AC FWHM of 150 fs corresponding to a pulse duration of 97 fs was only 7 % above Fourier-limit and therefore indicates that the pulse chirp mainly linearly decreases during the propagation in the amplification fiber. The pulse duration after amplification is about halved compared to the Fourier-limited seed pulse duration of 220 fs and thus was even shorter than the pulse of 108 fs duration demonstrated by Imeshev and Fermann, although the Fourier-limited

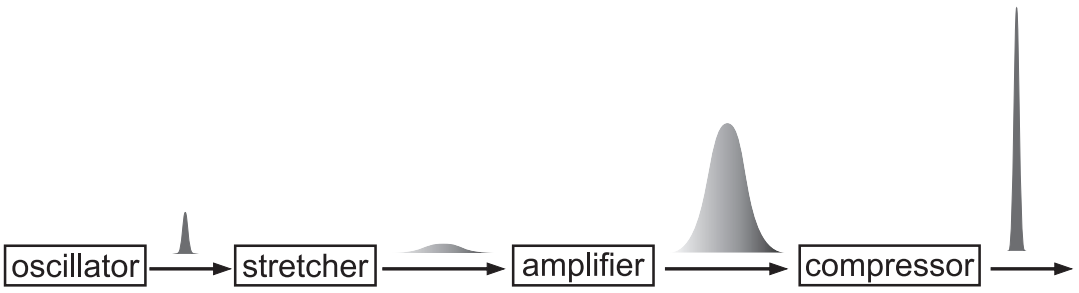

Figure 4.3: Schematic of a CPA-Setup

seed pulse duration had been more than 50 % larger. However, with 644 mW average output power corresponding to 17 nJ of pulse energy, both average output power and pulse energy were significantly lower. Increasing the pump power was not appropriate, since it did not lead to further pulse shortening, but to an increasing FWHM of the AC trace and the occurrence of a pedestal. This could not be balanced by readjustment of the dispersion precompensation and therefore indicates that the pulse chirp becomes distorted due to soliton compression at the end of the fiber section. Hence, in contrast to the results by Imeshev and Fermann [11], the pulse energy was not limited by pump power, but by nonlinearity.

4.2 Chirped-pulse amplification

In order to overcome the nonlinear pulse energy limitation and generate pulses with megawatt (MW) or even higher peak powers, chirped pulse amplification has proven to be an adequate approach. As mentioned before, the concept of CPA is to reduce peak intensity by dispersively stretching the pulses before the amplification process and recompress them afterwards. This procedure is sketched in Fig. 4.3. In principle, if the stretching ratio is large enough, the peak intensity can become indefinitely low, so that very large amplification with negligible nonlinear influence can be realized.
However, if gratings are used for pulse stretching or compression, the stretching ratio as well as the maximum peak intensity after recompression are limited by the free aperture of the gratings due to the spatial expansion of the spectrally chirped pulses and their damage threshold. Furthermore, the impact of higher order dispersion mismatch on

the pulse recompression increases with the stretching ratio. If fibers are used for pulse stretching, which is the case in the present work, especially the latter aspect becomes more relevant, as typically fiber dispersion does not perfectly match the dispersion of a compressor based on gratings.

4.2.1 Experimental setup

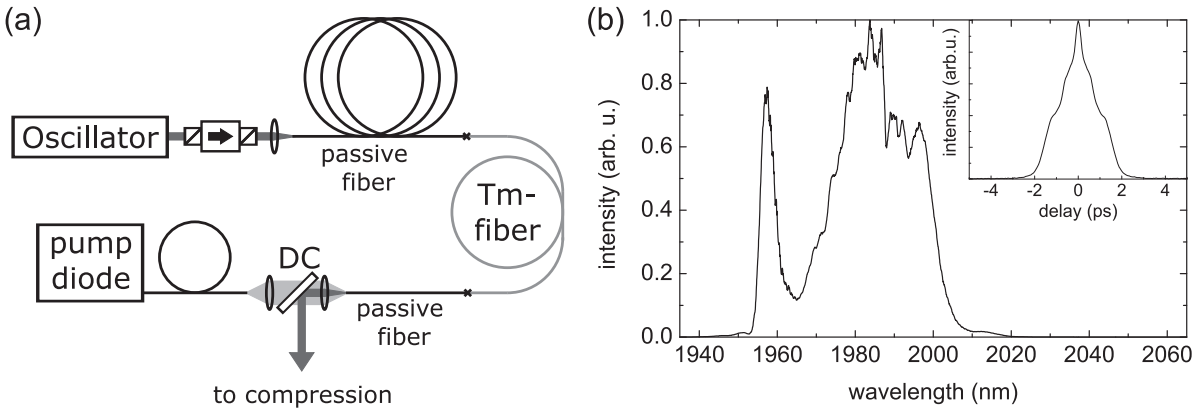

Figure 4.4: (a) Schematic of the experimental setup; DC: dichroic mirror. (b) Optical spectrum and AC trace (inset) of the seed oscillator.

The CPA setup is based on the configuration presented in section 4.1.1. Instead of the grating arrangement, 10 m of passive double-clad LMA fiber with the same core and cladding diameter and NA were spliced to the active fiber, providing about -0.9 ps^2 of GDD for additionally chirping the seed pulses. The active fiber was shortened from 2.8 m to about 2.75 m during splicing the fiber section.

Pulse recompression after amplification was realized by a grating configuration providing about 1.3 ps^2 of GDD. Due to the large core diameter of the applied fibers, waveguide dispersion could be neglected. Assuming the third order dispersion of fused silica for the fiber section, the residual third order dispersion (TOD) after the compressor was 1.4×10^{-3} ps^3 for perfectly matched GDD of fiber section and compressor. Higher order dispersion terms have not been taken into account.

As seed source, the laser described in chapter 3 was used. The optical spectrum and AC trace of the seed pulses are displayed in Fig. 4.4 (b). The RMS width of 13.2 nm

at a center wavelength of 1980 nm corresponds to a Fourier-limited pulse duration of 195 fs. The pulses were negatively chirped to a duration of about 700 to 800 fs. The seed pulse energy after the isolator was 3.3 nJ at the fundamental repetition rate of 37.6 MHz corresponding to an average power of 124 mW.

4.2.2 Amplification results

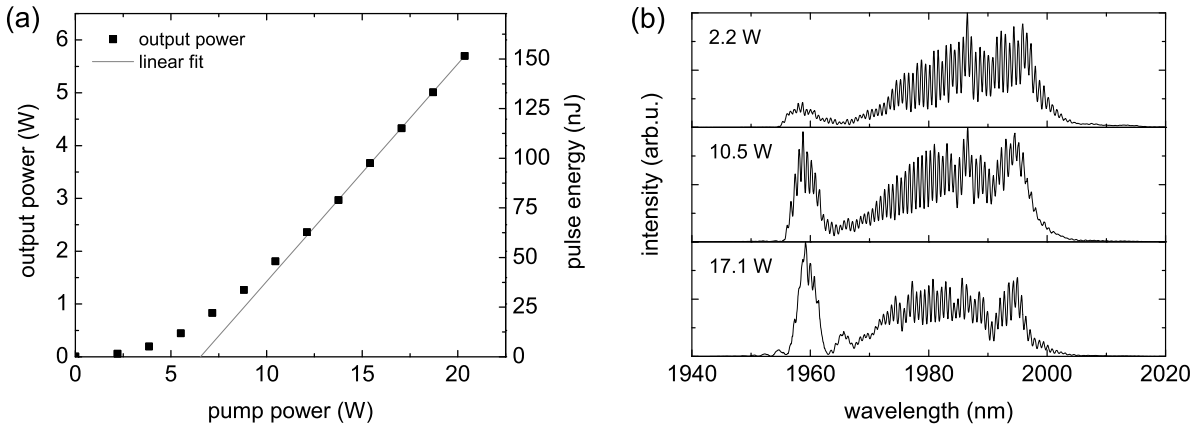

Figure 4.5: (a) Amplifier output power and corresponding pulse energy versus pump power launched into the fiber. The linear fit corresponds to a maximum slope efficiency of 41 %. (b) Selected optical spectra at different pump power levels.

Pump power variation

Fig. 4.5 (a) shows the amplifier average output power and the corresponding pulse energy versus pump power. Below about 12 W of launched pump power, a non-constant slope can be recognized. According to the fiber emission cross section, the saturation power at 1980 nm is 371 mW. Since the launched seed power was significantly lower and was furthermore partly absorbed at the beginning of the amplification fiber section, the absorbed pump power could not be efficiently extracted at lower levels, which is the main reason for the increasing slope. A further contribution reducing the efficiency results from the 3-level-structure of thulium at 1980 nm [15]. The population of the lower laser level requires a certain amount of pump power to achieve population inversion. However, since the seed oscillator is operated with even lower pump power this effect is regarded

to be of minor influence.

Above 12 W of pump power launched into the fiber and 2.5 W of average output power, the amplification became saturated and a maximum slope efficiency of 41 % was achieved, which corresponds to the quantum limit between pump and emission wavelength. As there are always some parasitic effects lowering the conversion efficiency, a quantum limited efficiency indicates some non negligible influence of cross relaxation. As mentioned in section 2.1, the cross relaxation process enables to get more than one excited thulium atom per absorbed pump photon, when thulium is pumped at 793 nm [38]. Assuming a quantum efficiency of 1.3, which was given by the fiber manufacturer, the maximum possible slope efficiency is 52 %. A slope efficiency of 41 % therefore corresponds to an excited state to photon conversion efficiency of 79 %, which is still a very good value. The maximum output power of 5.7 W corresponding to 151 nJ of pulse energy was limited by the available pump power.

In Fig. 4.5 (b), the spectral evolution with increasing pump power is displayed by selected spectra. For lower pump powers, the peak at the short wavelength side of the spectrum is significantly lower compared to the seed spectrum and increases with launched pump power, until it even exceeds the main peak at higher pump power. Consequently, the central wavelength shifts to shorter wavelengths. This can be attributed to the 3-level nature of thulium in this wavelength region. At low pump power, significant losses especially for shorter wavelengths are introduced by reabsorption of the weakly pumped fiber segment (compare section (3.1)). With increasing pump power, these reabsorption losses are reduced and the central wavelength of the gain spectrum shifts to shorter wavelengths. As a result, the central wavelength of the amplifier output spectrum also shifts and the sidepeak becomes more dominant.

During amplification the spectral RMS width slightly decreased. This decrease depended on the output power, but occurred at any power level and, hence, can be attributed to several effects, for which the respective contribution could not be separated. One of these effects is the influence of SPM, which in combination with negatively chirped pulses leads to a reduction of the spectral width. Since no significant nonlinear deformation of the

spectral shape could be observed, the nonlinearity is estimated to be of minor influence. Nevertheless, some reduction of the width may occur at the beginning of the stretching fiber, at which the pulse is still relatively short, as well as at the end of the amplification fiber, at which the pulse energy is relatively high. While the first effect is of course independent of the amplification, the latter one depends on the respective pulse energy. Furthermore, the spectral width is reduced due to linear effects like gain narrowing and a mismatch of the center wavelength of pulse and gain spectrum.

Even if the influence of fiber nonlinearity is considered to be relatively low, it is not completely eliminated. Above about 11 W of launched pump power, increasing sidelobes around the short wavelength peak can be found. Due to the large pulse chirping, the spectral shape translates to the pulse in the time-domain. Therefore, the peak on the short wavelength side of the spectrum can be found at the leading edge of the temporal pulse. Consequently, the influence of fiber nonlinearity becomes visible here first, leading to sidelobe generation.

However, these sidelobes did not have any distinct effect on the pulse quality. The FWHM of the measured AC traces after the amplifier was about 25 ps. Below the maximum launched pump power, the pulses could be recompressed to about 10 to 15 % above Fourier-limit, revealing no significant degradation of pulse quality. The residual deviation can mainly be attributed to the mismatch of TOD of the amplifier fiber section and the grating compressor.

Maximum output pulse energy

The spectral and temporal output characteristic at the maximum launched pump power of 20.4 W are displayed in Fig 4.6. Fig 4.6 (a) shows the measured (black continuous curves) and calculated (grey dashed curves) AC traces before (inset) and after recompression. The measured AC trace of the uncompressed pulse with a FWHM of about 25 ps agrees well with one calculated from the output spectrum (Fig. 4.6 (b)) assuming a chirp of -1.3 ps^2. The pulses could be dechirped to an AC FWHM of 364 fs corresponding to 256 fs of pulse duration, which was 17 % above bandwidth-limit. The pedestal in the AC trace and the FWHM were slightly increased compared to lower pump powers.

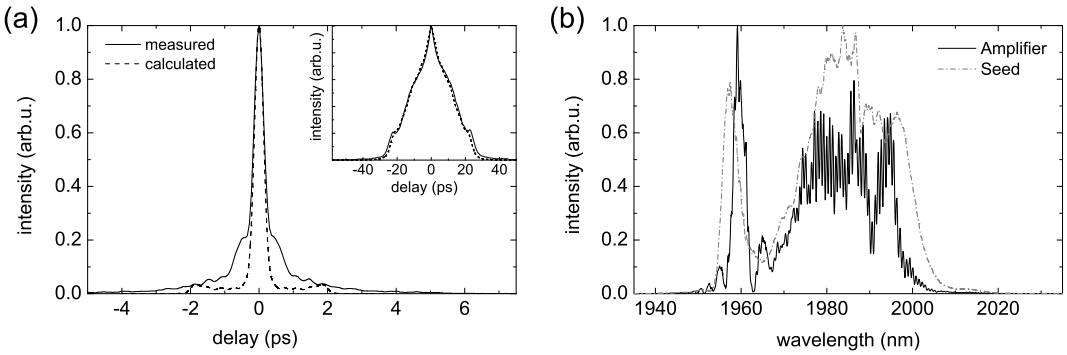

Figure 4.6: Amplifier output (a): AC trace of the compressed (continuous curve) and Fourier-limited pulse (dashed curve); inset: measured AC trace of the uncompressed pulse (continuous curve) and calculated AC trace (dashed curve) assuming a spectral chirp of -1.3 ps^2; (b): Spectrum before (dashed grey curve) and after amplification (continuous black curve).

The increase of the AC FWHM could not be balanced by readjustment of the grating distance and therefore is an indication for the beginning influence of nonlinearity on the pulse. The B-integral was estimated to be $< \pi$ using numerical simulations.

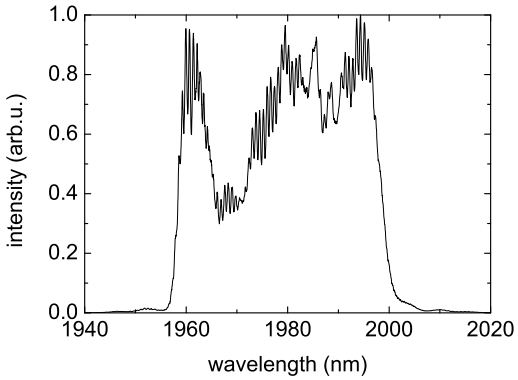

Figure 4.7: Spectrum after amplification with single-mode fiber pigtail.

The oscillations in the spectra with a fringe distance of 0.7 nm resulted from interference between the fundamental mode and a higher transversal mode. With a V number of 3.97, the applied fibers are not exactly single-mode, but also support propagation of the LP11 as well as the LP21 and LP02 mode. The latter ones are estimated to play no significant role as they propagate mainly in the cladding at the given V number and therefore should be sufficiently suppressed by coiling the fiber [39]. For the stretching fiber, excitation of the LP11 mode can be prevented by proper alignment of the freespace

coupling: However, at the transition to the active fiber segment it basically depends of the quality of the splice.

The slightly different effective refractive index of the transversal modes leads to a temporal delay, which becomes apparent in the spectral modulations. This explanation was supported also by calculations of the propagation constants of the respective modes. From the modulation depth measured with a multimode fiber the power content in the higher mode was estimated to be less than 30 %.

This explanation could further be verified by splicing a short piece of single-mode fiber (≈ 0.4 m) to the end of the fiber section, which led to a significant decrease of the spectral modulation depth. A representative spectrum is shown in Fig. 4.7. Bending of the fibers actually did not result in any significant improvement, which could be due to the short length of the single-mode fiber. By increasing the length of the fiber pigtail one would expect a higher propagation loss of the higher mode and therefore a better beam quality and a decreasing modulation depth. On the other hand, as the mode-field diameters of the active and the passive fiber are not perfectly matched, implementation of single-mode fiber also introduces some additional splicing loss for the fundamental mode and thus also lowers the fundamental mode output power. Furthermore, at least the applied fiber is not suitable for complete removal of the oscillations, since it also is a double-clad fiber and therefore the higher transversal modes removed from the signal core are still guided by the pump cladding. Consequently, the spatial overlap of the modes and thus the depth of the modulation fringes is reduced due to the significantly higher NA of the pump cladding, but is not completely eliminated.

4.3 Conclusion

In this chapter, two different concepts of pulse energy scaling with thulium-doped fibers were evaluated. By positively prechirping the pulses, shortening of the pulse duration from 220 fs to 97 fs and a maximum output power of 644 mW, corresponding to 17 nJ of pulse energy with no subsequent pulse recompression could be achieved. However, the pulse energy was limited by excessive accumulation of nonlinear phase.

As an alternative approach, the pulses were amplified in a CPA scheme. To the author's knowledge, this was the first time that this concept was applied for ultra-short pulse amplification in the 2 µm spectral region. A maximum average output power of 5.7 W, corresponding to 151 nJ of pulse energy could be achieved. Both values represent a record in the amplification of ultrashort pulses with thulium-doped fibers. Although some influence of nonlinearity on the pulse could be observed, the output power was limited by available pump power. Due to linear and nonlinear effects, the Fourier-limited pulse duration increased from 195 fs to 219 fs during amplification. Nevertheless, the pulses still could be compressed to 256 fs, which was 17 % above Fourier-limit.
After the amplification process, spectral modulations with a fringe distance of 0.7 nm were observed. These resulted from interference between LP01 and the LP11 transversal mode. The power content in the LP11 mode was estimated to be less than 30 %.
In order to avoid the spectral modulations and to improve the beam quality of the amplified pulses, truly single-mode fibers should be applied. Meanwhile, diode lasers with a core diameter of 100 µm and up to 35 W of output power at 793 nm wavelength are commercially available. The beam quality of this pump sources is sufficient for efficient amplification at 2 µm wavelength in thulium-doped single-mode double-clad fibers with 125 µm diameter. However, due to the smaller mode-field area (MFA) in this fibers, the pulse stretching needs to be increased in order to avoid excessive nonlinear phase contributions, which requires careful dispersion management to maintain a good pulse compressibility.

5 Oscillators with fiber dispersion management

In chapter 2 it was described that the waveguide properties of single-mode fibers introduce positive GVD and consequently shift the point of zero GVD towards longer wavelength. With proper fiber parameters it is possible to shift this point even beyond 2 µm wavelength and thus to achieve normal GVD in this spectral region. Such fibers are suitable to implement normal dispersion in thulium-doped ultrashort pulse fiber lasers and thus enable fiber-integrated dispersion management.

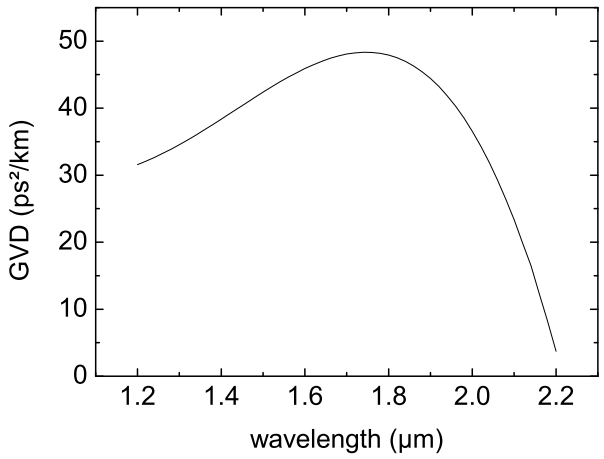

Figure 5.1: GVD of the normal dispersion fiber (NDF).

In this work, a fiber with a NA of 0.28 and a cutoff-wavelength of 1 µm, corresponding to a core diameter of 2.75 µm, was used for the implementation of normal dispersion into ultrashort pulse fiber laser cavities. The GVD of this fiber, derived from these parameters, is displayed in Fig. 5.1.

In preliminary experiments this fiber was used to adapt the pulse parameters of a laser operating in the fundamental soliton regime via partly compensating for the cavity GDD. The corresponding results are presented in section 5.1.

Overcompensation of the anomalous cavity GDD enabled operation of the laser in the

PCP regime. The experimental results and numerical investigations are presented in section 5.2.

5.1 Soliton fiber laser

Starting point for the investigations with the normal dispersion fiber (NDF) was a laser containing only fibers with anomalous GDD and thus operating in the fundamental soliton regime. The setup is sketched in Fig. 5.2 (a).

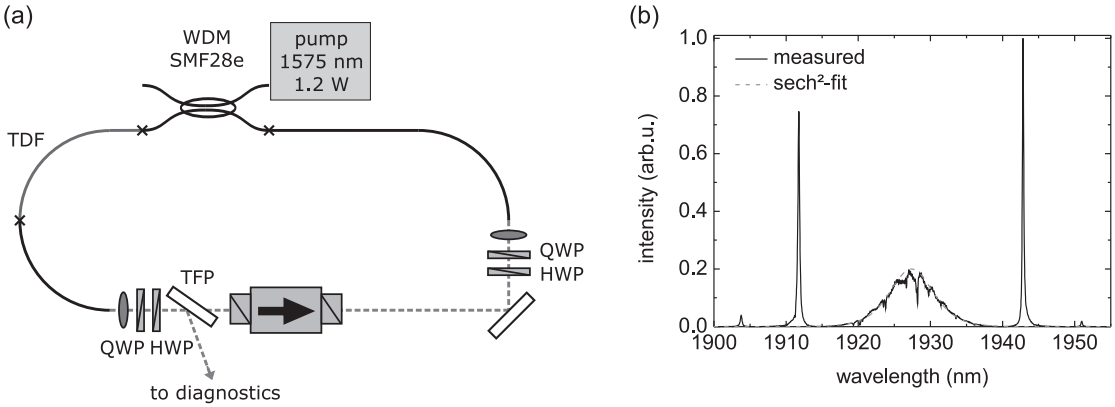

Figure 5.2: (a) Setup of the soliton fiber laser. TDF: thulium-doped fiber, TFP: thin-film polarizer, HWP: half wave-plate, QWP: quarter wave-plate; (b) Optical output spectrum of the laser.

The laser was arranged in a ring resonator configuration and was mode-locked via NPE. The active fiber was a 0.9 m long thulium-doped fiber (TDF) with a cutoff wavelength of 1350 nm and 0.26 NA, as given by the fiber manufacturer. It was pumped at 1575 nm with a maximum pump power of about 1.2 W via a 1575/1970 nm WDM made of standard SMF28e fiber. Two pigtails of a single-mode fiber with 7 µm core diameter and 0.2 NA at both ends of the fiber section were used to adapt the respective mode-field diameters. The GDD of the applied fibers sums up to about -0.18 ps^2.

The free-space section contained several waveplates for polarization adjustment, a TFP in Brewster's angle, which was used as polarization selective element and also acted as an output coupler, followed by an isolator to ensure the unidirectional operation.

With the waveplates set appropriately, the mode-locking was self-starting at about

300 mW of launched pump power. The pump power could then be reduced to about 115 mW for single-pulse operation with 12 mW of average output power corresponding to 185 pJ of single-pulse energy at the fundamental repetition rate of 64.8 MHz. The optical spectrum is displayed in Fig. 5.2 (b). It is centered at 1927 nm with distinct Kelly-sidebands, which contain about 25 % of the pulse energy and strongly indicate operation in the fundamental soliton regime. The spectral FWHM of about 7 nm corresponds to 555 fs of Fourier-limited pulse duration. However, the pulse intensity was not sufficient to align an autocorrelator for measurement of the actual pulse duration and verification of single pulse operation. Nevertheless, as neither the optical spectrum nor measurement of the pulse train or the radio-frequency spectrum revealed any indications for multiple pulse operation, the laser was expected to operate in the single-pulse regime. The spectrum shows sharp cuts, which are irregularly distributed over the entire width. The shape indicates that they are caused by absorption lines of atmospheric molecules, especially water, which are very pronounced in this wavelength region [40]. Such cuts could also be observed with measurements of amplified spontaneous emission (ASE), in which the fiber was directly connected to the optical spectrum analyzer (OSA) without any freespace sections. Therefore and for the reason that no relation between the depth of the cuts and the length of any freespace section could be found, neither cavity-internal nor external, it can be assumed that the molecules are already contained inside the fibers itself and the absorption bands are not necessarily related to the freespace section inside the laser cavity.

Hybridly mode-locked soliton setup

In the next step, the cavity was extended by a SBR in a sigma-arm configuration, which was implemented after the isolator in the backcoupling path of the freespace section. The unsaturated loss, modulation depth and a saturation fluence of the SBR at 1960 nm were specified by the manufacturer with 30 %, 18 % as well as 130 µJ/cm^2, respectively. With this additional stabilization, single pulse mode-locking could be directly observed at about 100 mW of launched pump power. The output pulse energy could be increased to 250 pJ, where the Kelly-sidebands contained about 30 % of the energy.

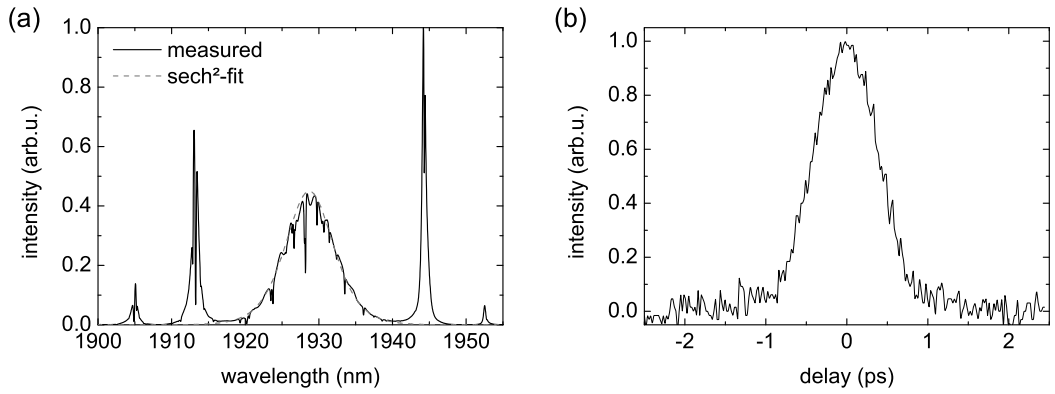

Figure 5.3: (a) Optical spectrum and (b) AC trace of the soliton fiber laser hybridly mode-locked via NPE and SBR.

This pulse energy was sufficient for alignment of the autocorrelator and verification of single-pulse operation. The corresponding optical spectrum and autocorrelation trace are shown in Fig. 5.3. The spectrum is again centered at around 1930 nm with a slightly increased FWHM of 7.7 nm. The half-width of 937 fs of the AC trace corresponds to 612 fs pulse duration, assuming a sech^2 pulse shape, which was 20 % above the Fourier-limited pulse duration of 510 fs.

The increased pulse energy compared to the laser purely mode-locked by NPE is mainly attributed to a higher outcoupling ratio. Even with pure NPE mode-locking the pulse energy could be increased to more than 200 pJ by adjusting the waveplates during mode-locked operation. However, with higher outcoupling ratio the mode-locking threshold also increased until self-starting could not be achieved with the respective waveplates setting. Since the additional SBR efficiently discriminates CW against pulsed operation, self-starting could be maintained at higher outcoupling ratios, and consequently higher output pulse energies could be delivered.

Dispersion variation

For the following experiments, a piece of NDF was implemented into the fiber section to partly compensate for the GDD of the anomalous dispersive fiber section. To investigate the influence of the normal dispersion segment on the output pulse parameters, the length of NDF was subsequently reduced from 0.73 m to 0.07 m. In Fig. 5.4 (b), the

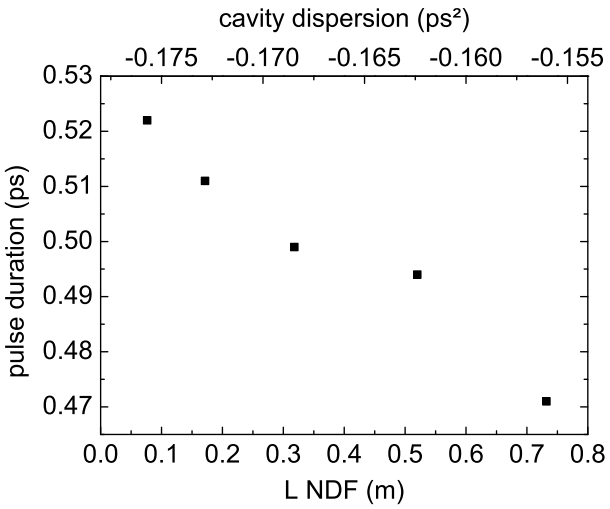

Figure 5.4: Fourier-limited pulse duration vs. length of the NDF/cavity dispersion.

Fourier-limited duration of the output pulses is plotted versus the length of the NDF. As expected, increasing the NDF fiber length and thus reducing the cavity GDD led to an increase of the spectral width and consequently to a decrease of the Fourier-limited pulse duration from about 0.52 to 0.47 ps. Owing to the soliton area theorem, a shorter pulse duration is expected to be accompanied by a higher pulse energy. However, as the quality of the fiber splices and the waveplates position were not optimized for maximum output pulse energy at each fiber length and therefore the pulse energy randomly varied with the cavity dispersion, this relation could not be confirmed. Nevertheless, this results verify that the applied fiber is suitable for fiber laser dispersion management in the 2 µm spectral region.

5.2 Positively chirped pulse operation

In contrast to the grating arrangement applied for dispersion management in section 3, the NDF cannot only be used to implement normal GVD, but also provides nonlinearity on the normal dispersion section. As mentioned in section 2.3, the combination of normal GVD, SPM and optical gain linearizes the chirp of a positively chirped pulse and is therefore necessary for PCP in fiber lasers. On the premise that the gain can separately be provided by an anomalous GVD fiber, the NDF therefore enables the

transfer of monotonically positively chirped pulse operation schemes from ytterbium and erbium to thulium-doped fiber lasers.

5.2.1 Experimental investigations of the single pulse operation

In this section, experimental investigations on single pulse operation of a thulium-doped fiber laser with a NDF for dispersion management and positive cavity GDD are presented.

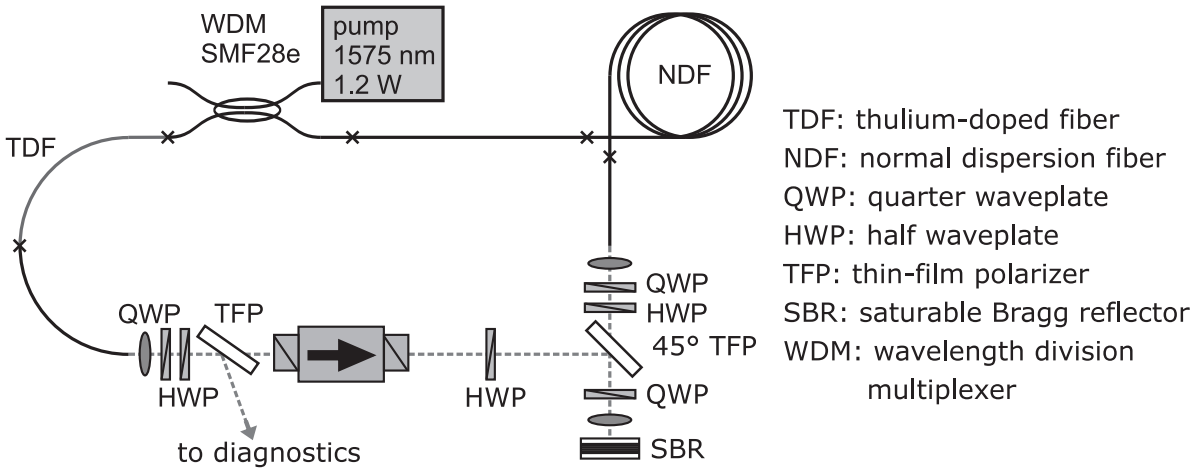

Figure 5.5: Experimental setup of the thulium-doped PCP fiber laser.

Experimental setup

The experimental setup is shown in Fig. 5.5. For large parts, it corresponds to the setup of the soliton fiber laser depicted in Fig. 5.2 (a). The extended freespace section includes the additional σ-arm consisting of a TFP under an angle of 45°, the SBR with a focussing lens and a half waveplate (HWP) as well as a quarter waveplate (QWP) to adjust the polarization. The NDF with a length of 6.6 m was inserted into the single-mode fiber (SMF) pigtail at the backcoupling part of the fiber section before the pump WDM, resulting in a cavity GDD of 0.04 ps^2 at 1930 nm, which was determined via measurements of the frequency-dependent group delay. The fundamental repetition rate was 19.7 MHz.

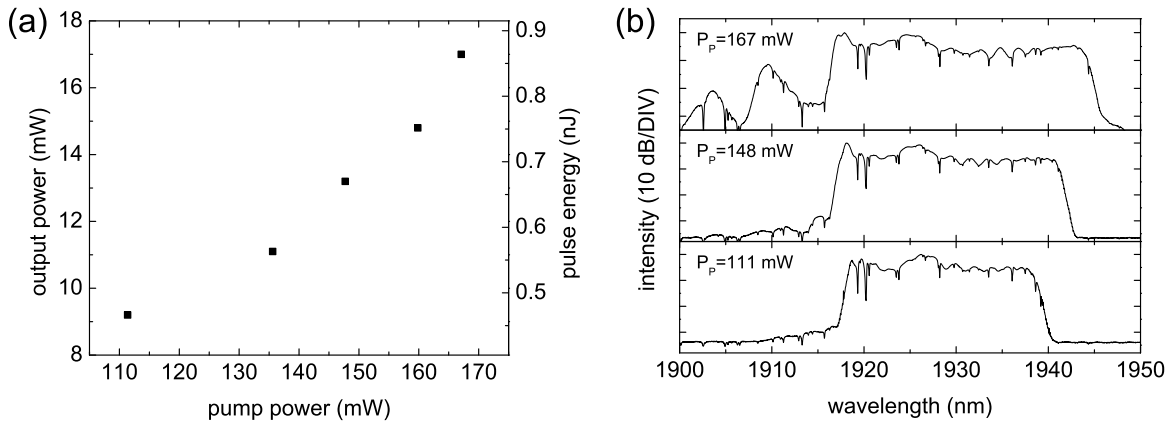

Figure 5.6: (a) Average output power and pulse energy vs. pump power; (b) Optical spectra at different pump power levels.

Experimental results

Mode-locked operation was self-starting at about 110 mW of launched pump power. In Fig. 5.6, the average output power and pulse energy vs. pump power as well as several corresponding output spectra at different pump power levels are displayed. The average output power in single-pulse operation almost linearly varied with the pump power between about 9 and 17 mW.

The spectra, centered at around 1927 nm, are characterized by a mainly rectangular shape with sharp edges,which are typical for PCP [41]. Two peaks appear around the center and on the short wavelength side at about 1917 nm wavelength.

With increasing pulse energy, the spectrum monotonically broadens from about 20 to 28 nm at -10 dB while mainly maintaining its shape. The Fourier-limited pulse duration reduces from 489 to 324 fs. However, above about 160 mW of pump power, sidelobes appear on the short wavelength side. In addition, a small bump can be found on the long wavelength side.

During variation of the pump power, the autocorrelation trace of the pulses directly from the laser remained mainly unchanged. In Fig 5.7 (a), a representative AC trace measured at 148 mW of launched pump power is shown. The FWHM is about 15 ps, indicating a large pulse chirp.

The pulses could externally be dechirped with a standard grating compressor providing

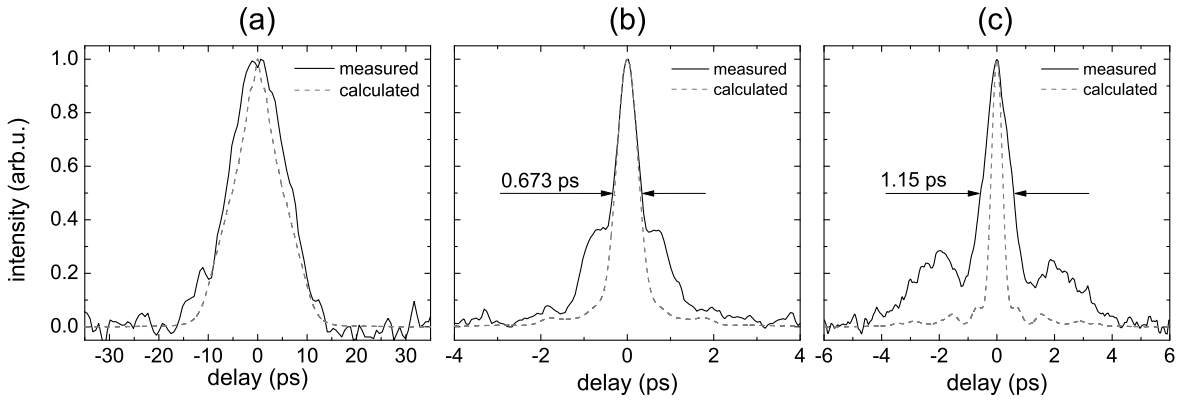

Figure 5.7: Autocorrelation traces before (a) and after compression (b) and (c). The measurements are depicted with the black continuous curve, the dashed grey curves indicate calculated AC traces assuming a pulse chirp of 1.04 ps^2 (a) and a Fourier-limited pulse, (b) and (c), respectively.

about -1.04 ps^2 of GDD. The resulting AC traces of the recompressed pulses at a pump power of 148 and 167 mW are shown in Fig. 5.7 (b) and (c), respectively. At 148 mW of launched pump power, the pulses could be dechirped to a duration of 482 fs, which was only 13 % above Fourier-limit and thus reveals a mainly linear pulse chirp. However, with increasing pump power, significant side-lobes appeared in the AC trace indicating deviations from the linear pulse chirp, which thus cannot be balanced by the grating compressor. With larger pump power levels, the side-bumps progressively separated from the main pulse. Furthermore, at 167 mW of launched pump power the pulses could not be recompressed to less than about a factor of two above Fourier-limit. Further increase of pump power led to destabilization of the operation, revealed by side-bands in the RF-spectrum, and an irregular pulse train and finally to a complete break-up of the pulses.

Discussion of the experimental results

According to the experimental results, a number of similarities to the well known PCP schemes at 1 µm can be found, especially to the similariton regime. The GDD required for pulse compression is about 5 times larger than the combined GDD of the anomalous fiber segments inside the cavity. Therefore, it can be concluded that the pulse is positively chirped during the entire resonator roundtrip and hence is operating in a PCP regime.

Nevertheless, it can be well compressed with a standard grating compressor indicating a very smooth quadratic phase. The spectral width scales almost linearly with the pulse energy while maintaining its shape, which is characterized by a mainly flat profile with steep edges that are very typical for PCP schemes.

However, in lasers, in which the GVD is normal for all applied fibers, significantly larger pulse energies are routinely observed, which are mostly limited by multiple pulse operation due to overdriving of the saturable absorber mechanism [42]. With the present setup, the pulse quality strongly degrades at larger pulse energy revealed by incompressible side-lobes in the autocorrelation trace and increasing deviations from the Fourier-limited pulse duration. Simultaneously, the spectrum develops side-peaks on the short wavelength side. Further increase of the pump power finally leads to complete break-up of the pulses. These observations indicate that the pulse limitation is inherent to the propagation itself.

Two approaches are considered to provide a potential explanation for these phenomena. A significant difference between the laser presented here and similar setups in other spectral regions is the anomalous GVD of the amplification fiber. In section 2.3.3 it was mentioned that the combination of normal GVD and SPM in the presence of optical gain balances spectral phase contributions on a positively chirped pulse, linearizes the pulse chirp and thus, as long as the nonlinearity does not become excessive, provides stabilization of the pulse propagation. Contrary to this, the contributions of anomalous GVD and SPM both reduce the chirp and therefore lead to distortions in the pulse shape and accordingly in the spectral phase [23]. In the present setup, the amplification and the segment providing nonlinearity in combination with normal GDD are spatially separated. The pulse reaches its maximum energy and is close to its minimum duration after the thulium-doped fiber in the following passive fiber pigtail. Therefore, it can be estimated that these fiber sections provide large contributions on the pulse shaping. If these become predominant over the linearization of the chirp in the normal GVD fiber segment, the pulse propagation destabilizes.

Modulation instability (MI) provides a further explanation for the limited pulse energy.

Several publications show that MI can also occur in fiber systems with periodic dispersion variation, even if the net dispersion is normal [43, 44, 45]. The frequency of the maximum MI gain of the first sideband is then given by [44]:

$$\Omega_{max} = \sqrt{\frac{\frac{2\pi}{L} - 2\gamma P_0}{4\pi^2 \beta_{av}}} \tag{5.1}$$

where L denotes the length of fiber link period, P_0 the signal power and β_{av} the average GVD. Due to fiber birefringence, the boundary condition of a cavity enables modulation instability (MI), even if the fiber GVD is completely normal [46]. In a very recent publication, MI has been observed and studied in a dissipative soliton fiber laser [47].

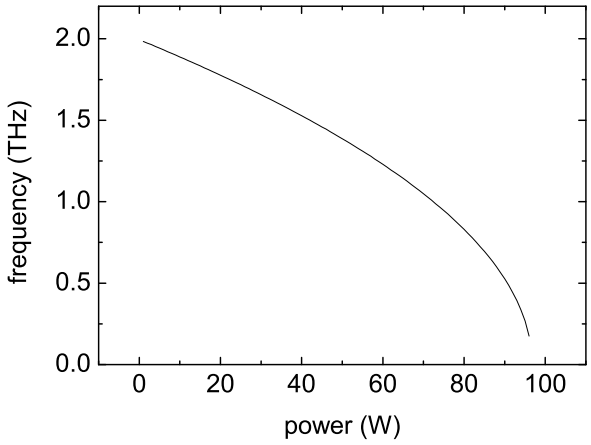

Figure 5.8: Frequency of the maximum first order MI sideband gain versus power calculated according to [45].

The argument for MI as the limiting effect is indicated by the occurrence of the sidebands in the optical spectrum at large pulse energies. Their structure conspicuously agrees with the spectral sidebands observed by Peng et al. [47]. Furthermore, the pedestal revealed in the corresponding AC traces was attributed to the induced sidebands. In Fig. 5.8, the frequency of the maximum first order MI gain at a wavelength of 1930 nm is plotted versus power according to equation (5.1) assuming a fiber length of 12 m and an average GDD of 0.04 ps^2. The frequency distance of about 600 GHz between the sidebands in Fig. 5.6 agrees reasonably well with the values expected corresponding to the power levels

inside the oscillator and thus supports this explanation.

5.2.2 Numerical investigations of the pulse propagation

In order to verify the experimentally observed pulse operation scheme and further investigate the cavity-internal pulse evolution and the limitations of the pulse parameters, numerical simulations were performed. Those were again carried out using the commercial software, which was also applied for the simulations presented in section 3.

Numerical Setup

The numerical setup is sketched in Fig. 5.9. The freespace section consists of the two saturable absorbers. The NPE absorber was implemented as a fast saturable absorber with transmission given by the reflectivity parameter $R = R_0 + \Delta R - \frac{\Delta R}{1+\frac{|A(T)|^2}{P_A}}$. The parameters were set to $R_0 = 5\,\%$, $\Delta R = 40\,\%$ and $P_A = 4\,\mathrm{W}$. The corresponding loss also includes linear losses introduced by further freespace elements like the fiber coupling and the isolator but excluding the SBR.

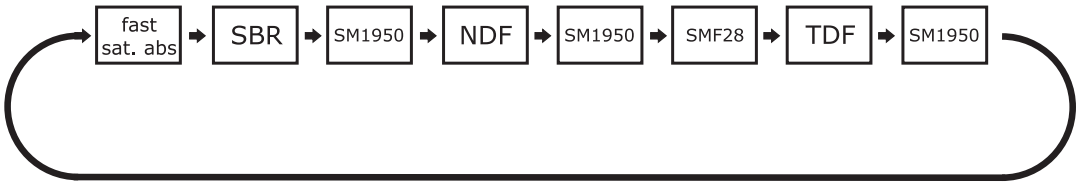

Figure 5.9: Schematic of the numerical simulation model.

After the fast saturable absorber the SBR was inserted with the parameters set correspondingly to the manufacturer's information: 70 % unsaturated reflectivity, 10 % saturable reflectivity, $130\,\mu\mathrm{J/cm^2}$ saturation fluence, 500 fs of relaxation time and a focal spot diameter of 8 µm.

The pulse propagation in the fiber section included the effects of SPM, self-steepening and Raman-response with the nonlinear refractive index set to $n_2 = 3.2 \cdot 10^{-20}\,\mathrm{m^2/W}$ and the Raman-coefficient set to 0.18. According to the parameters given by the fiber manufacturers, the mode-field diameter and GVD of the fiber segments were set to 8 µm and -74.24 $\mathrm{ps^2/km}$ for the SM1950, 7 µm and 42.57 $\mathrm{ps^2/km}$ for the NDF, 11 µm and

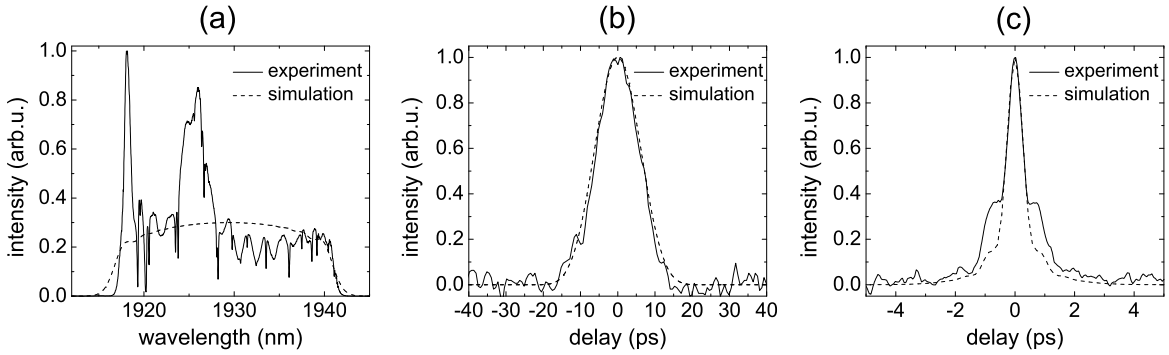

Figure 5.10: Experimentally observed (continuous curves) and simulated (dashed curves) pulse (a) optical spectrum and AC traces before (b) and after (c) compression.

-72.74 ps^2/km for the SMF28 and 6 µm and -23.73 ps^2/km for the TDF, respectively. The gain of the TDF was given by $g = \frac{g_0}{1+E/E_{Sat}}$ with $g_0 = 4\,m^{-1}$ and $E_{Sat} = 0.5\,nJ$. The spectral gain distribution was approximated by a Gaussian function with a FWHM of 75 nm at a center wavelength of 1929 nm.

Comparison of simulation and experiment

Fig. 5.10 reveals the very good agreement of the experimentally observed and the simulated pulses. The optical spectrum of the simulated pulses (Fig. 5.10 (a)) shows a mainly flat profile, while the edges are slightly less steep than the experimentally observed. The good agreement is confirmed by the Fourier-limited pulse durations of 431 fs and 426 fs in simulation and experiment, respectively.

The AC trace (Fig. 5.10 (b)) corresponds to an uncompressed pulse duration of 10.6 ps. The simulated pulses could be compressed to a pulse duration of 472 fs assuming a standard grating compressor corresponding to the experimental setup, which provided -1.13 ps^2 of GDD. The AC trace of the compressed pulse is displayed in Fig. 5.10 (c) and again is in very good agreement with the experiment.

The energy of the simulated pulses at the end of the fiber section was 1.7 nJ. Since the loss of about 1 nJ at the following fast saturable absorber also includes the other linear losses of the freespace section, this is also in very good agreement with the experimentally observed output pulse energy of 0.7 nJ.

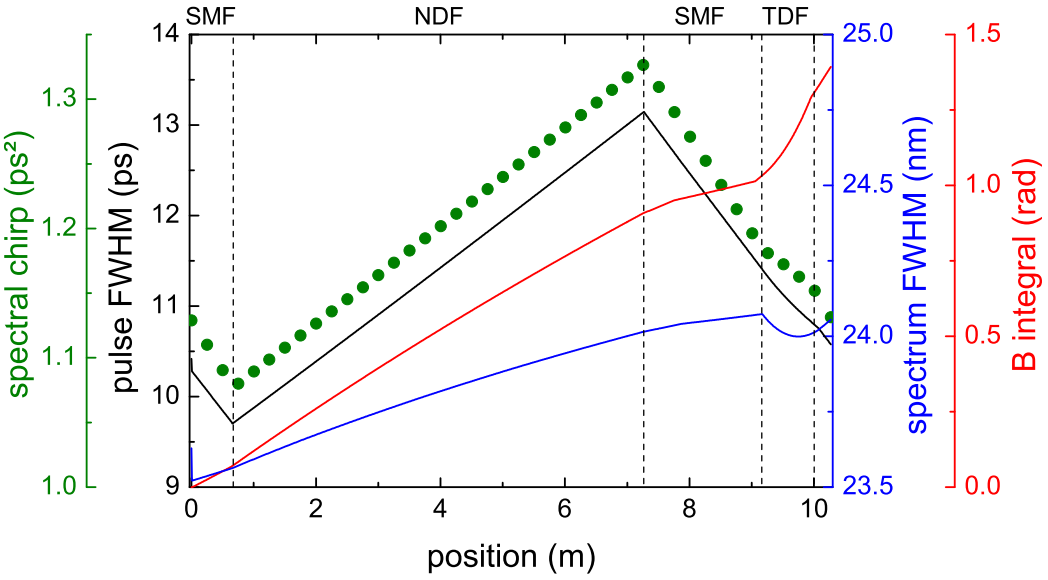

Figure 5.11: Pulse parameter versus resonator propagation: Temporal (black curve) and spectral (blue curve) pulse FWHM, pulse spectral chirp (green dots) and B integral (red curve); SMF: single-mode fiber, NDF: normal dispersion fiber, TDF: thulium-doped fiber.

Pulse propagation

The numerical reproduction of the experimentally observed pulses allows for deeper insight into the evolution of the pulse parameters during the resonator propagation. Fig. 5.11 shows the evolution of the temporal and spectral half-width (black/blue curve) as well as the pulse chirp and the accumulated nonlinear phase shift along a single resonator roundtrip. Corresponding to the GDD required for external pulse compression, the pulse is positively chirped during the entire cavity propagation. The pulse duration and chirp mainly alter linearly with the fiber dispersion. The spectral half-width nearly monotonically increases from about 23.5 to 24 nm during the fiber propagation due to the influence of SPM on the positively chirped pulse. Merely inside the TDF, gain narrowing leads to a slight decrease of the width until the increasing pulse energy again induces spectral broadening. Subsequently, the broadening is, due to the large chirp, reversed by temporal filtering with the saturable absorbers.

The evolution of these pulse parameters indicates that although the effect of fiber non-

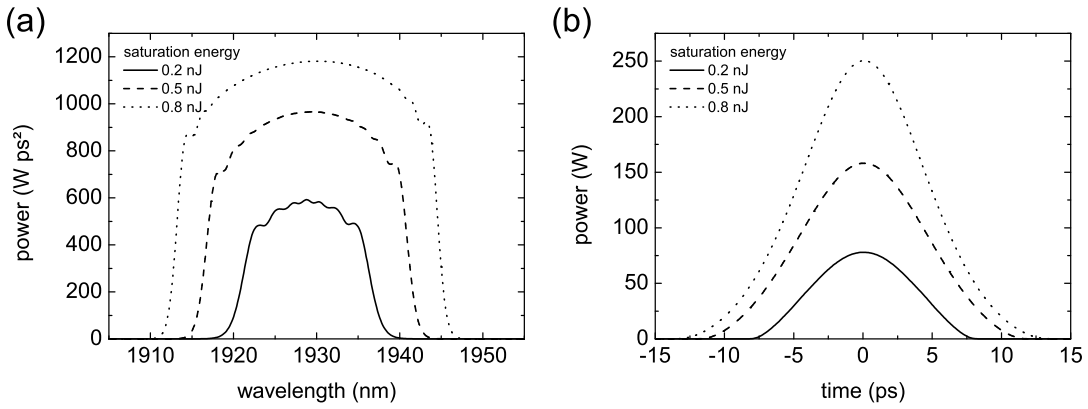

Figure 5.12: Pulse spectral (a) and temporal (b) shape for different saturation energies.

linearity on the pulse propagation is not negligible, it also does not play a very dominant role. The evolution of the pulse duration and spectral chirp does not reveal any significant nonlinear influence. Merely, the spectrum nonlinearly broadens during the propagation. However, this broadening is not very appreciable. The limited influence of the fiber nonlinearity is also confirmed by the accumulated nonlinear phase shift, which is with 1.35 rad relatively low for operation in the PCP regime. As stated in section 2.3, the pulse energy of ultrashort pulse fiber lasers is often limited by the maximum accumulated nonlinear phase shift, the pulse can tolerate. However, PCP schemes typically can tolerate very large accumulation of nonlinear phase. Therefore, further investigations are required to reveal the relation between the pulse energy and the stability of the laser operation.

Pulse energy variation

A very typical feature of PCP schemes is that the B integral and spectral bandwidth scale with the pulse energy or rather the applied pump power [48]. The corresponding relation between pulse energy and spectral bandwidth could also be observed experimentally (see section 5.2.1). To numerically verify these relations and further investigate the observed operation scheme, the saturation energy of the TDF was varied between 0.2 and 0.8 nJ while keeping the residual simulation parameters constant. Fig. 5.12 shows the spectral and temporal pulse shape for a saturation energy of 0.2, 0.5 and 0.8 nJ. As expected, the

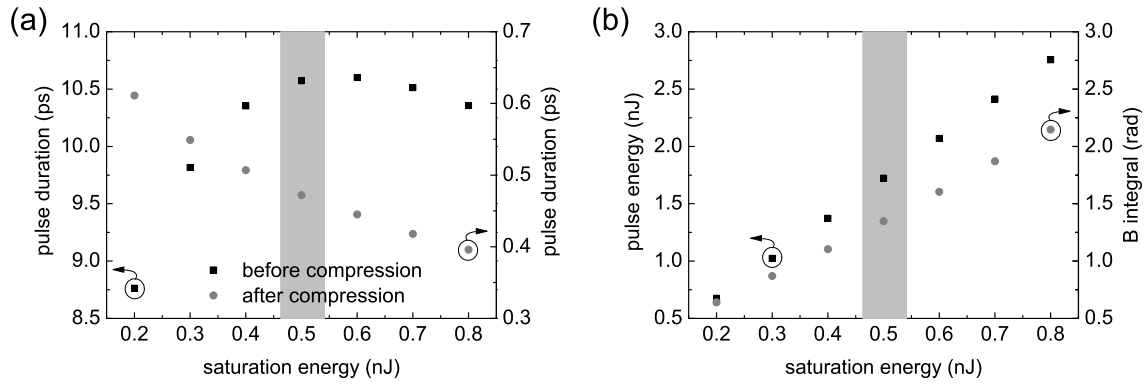

Figure 5.13: (a) Pulse energy (black squares) and B integral (grey circles) and (b) pulse duration before (black squares) and after (grey circles) compression versus saturation energy. The saturation energy of 0.5 nJ, with which the previous simulations have been performed with, is highlighted with the grey bar.

spectrum linearly scales with the pulse energy in width and power while maintaining its shape. The pulse duration, increases with the pulse energy in a low energy range and then slightly decreases at higher pulse energies.

The relation between pulse duration and energy is shown in more detail in Fig. 5.13 (a): The pulse duration reaches a maximum around 0.6 nJ of saturation energy and slightly reduces again for higher energies. The duration of the dechirped pulses, however, decreases with increasing saturation energy corresponding to the linear relation of spectral width and saturation energy. These results correspond to numerical simulations of an ultrashort pulse ytterbium fiber laser with dispersion-managed cavity operation in a PCP scheme, which were presented by Renninger et al. very recently [24]. Here, a monotonic increase of the spectral bandwidth with the pulse energy and an increase of the pulse duration for lower pulse energy as well as a slight decrease for larger pulse energy could be observed.

In Fig. 5.13 (b), the corresponding pulse energy and B integral are displayed. Both linearly increase with the saturation energy, but nevertheless with the maximum pulse energy of about 2.7 nJ and B integral of about $2/3\,\pi$ remain very low for a laser with a PCP scheme.

Above a saturation energy of 0.6 nJ, the steady state could not be achieved from quan-

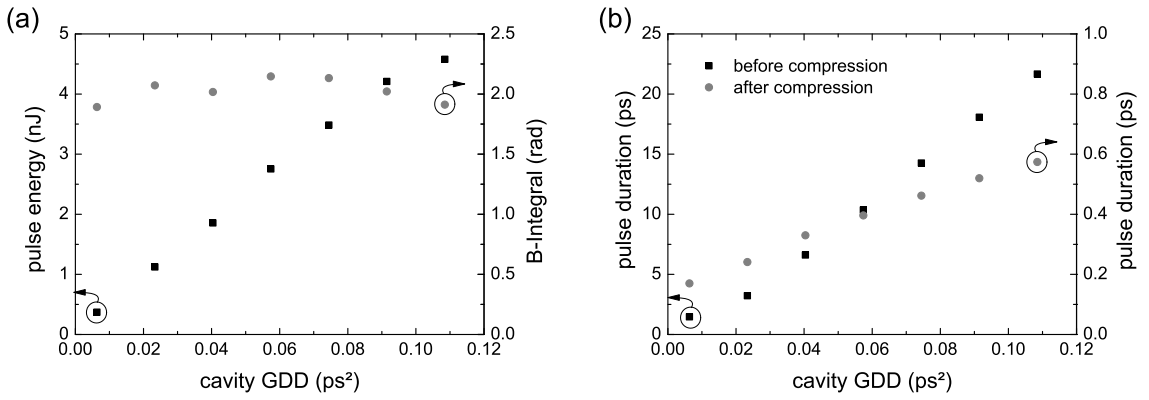

Figure 5.14: (a) Maximum pulse energy (black squares) and B integral (grey circles) and (b) pulse duration before and after (black squares) compression (grey circles) vs. GDD.

tum noise, but it was still stable versus small perturbations. With a saturation energy larger than 0.8 nJ, addition of quantum noise led to destabilization of the pulses within several resonator roundtrips. Since starting every single simulation from quantum noise would have been too time consuming, restabilization of the steady state after addition of quantum noise was chosen as stability criterion for these and the following simulations.

Dispersion variation

For most ultrashort pulse fiber lasers, the stability of the cavity-internal pulse propagation scheme imposes an upper limit on the energy of the propagating pulse. The cavity dispersion is a very relevant factor influencing the output parameters of an ultrashort pulse fiber laser. It was already mentioned that the pulse energy and the B integral in the presented system is relatively low for PCP. Therefore, variation of the cavity GDD can provide relevant information on the pulse energy limitation. Typically, a larger cavity GDD leads to increasing pulse energies, but is also accompanied by longer pulse durations [48, 49]. In order to verify this relation for the present system and to investigate the pulse energy limitation, the length of the NDF fiber was varied between 5.4 and 7.8 m, while the saturation energy each was adapted for maximum pulse energy.
In Fig. 5.14 (a), the pulse energy and B integral are plotted versus cavity dispersion; Fig. 5.14 (b) shows the pulse duration before and after compression. As expected, the

pulse energy as well as the pulse duration mainly linearly increase with the cavity GDD, while the temporal and spectral pulse shape do not significantly change over most of the parameter coverage. Merely at a very low cavity GDD of 0.006 ps^2, the spectrum deviates from the nearly rectangular shape.

At the minimum GDD of 0.006 ps^2, the pulses had an energy of about 350 pJ and a duration of 1.4 ps, which could be compressed to 170 fs by applying -0.067 ps^2 of GDD. The maximum pulse energy observed at 0.11 ps^2 of cavity GDD was 4.5 nJ with a pulse duration of 21.7 ps and 574 fs before and after applying -2.5 ps^2 of GDD for pulse compression, respectively.

However, the cavity B integral remained mainly constant, although the phase shift accumulated in the NDF linearly increased with the cavity GDD. This indicates that the pulse energy is not limited by the nonlinearity of the NDF, but by the overall nonlinear phase accumulation.

With a cavity dispersion of 0.006 ps^2 and saturation energy of 0.011 nJ, instead of PCP a stretched-pulse operation state could be observed without changing any of the other simulation parameters. Here, a significantly broader spectrum and shorter pulse duration as well as a larger B integral of 3.88 rad could be observed. Thus, the presented setup with the NDF for dispersion management is also suitable for stretched-pulse operation, which also has been demonstrated experimentally [50]. Nevertheless, with the saturation energy set to 0.012 nJ, the laser again operated in a PCP scheme with the pulse parameters given in Fig. 5.14. When the NDF length was reduced to below 5.2 m, resulting in an anomalous cavity dispersion, PCP could not be found.

These results indicate that PCP can be observed in thulium-doped fiber lasers even with very small normal GDD. With the cavity GDD close enough to zero, but still normal, the laser can be operated both with a PCP or a stretched-pulse operation scheme, while with anomalous GDD, no PCP but still stretched-pulse operation can be observed. This is also confirmed by the results presented by Gumenyuk et al., who observed PCP even when the cavity GDD was only slight normal, while with anomalous GDD the laser either operates in stretched-pulse or soliton regime [51].

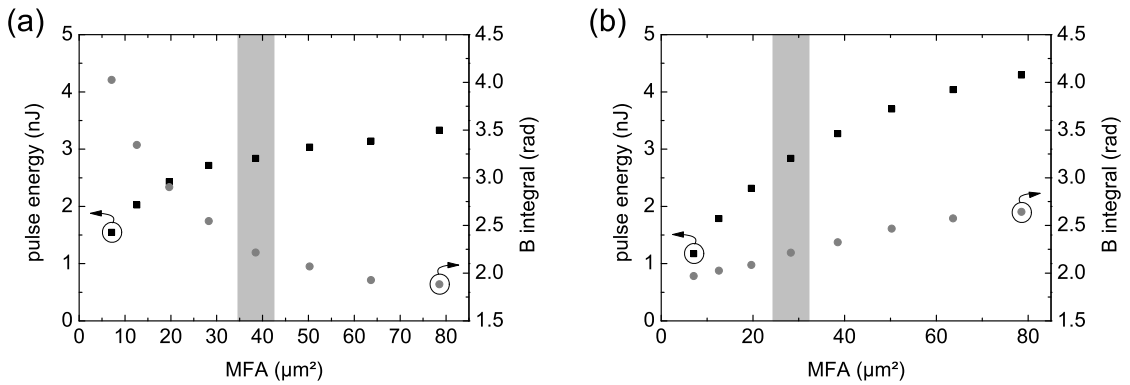

Figure 5.15: Maximum pulse energy (black squares) and B integral (grey circles) versus MFA of the (a) NDF and (b) TDF and the following standard fiber pigtail.

Pulse energy limitation

In every of the previous simulations of the PCP, the maximal nonlinear phase accumulated during a cavity roundtrip did not significantly exceed about $2/3\,\pi$. Presuming that the pulse energy is limited by a nonlinear effect, it needs to be investigated, if the limitation must be attributed to the total B integral accumulated over the entire cavity rountrip, like it appears from the cavity dispersion variation, or if it is related to the contribution of one of the fiber segments. According to Fig. 5.11, the standard fiber segments before and after the NDF only marginally contribute to the cavity nonlinearity, while most of the nonlinear phase-shift is accumulated along propagation in the NDF as well as in the TDF and the following standard fiber pigtail. Thus, it can be expected that the pulse energy limitation has to be attributed to one of these fiber segments. To investigate the influence of both of these segments on the pulse energy limitation, the mode-field area of the NDF and the TDF with the following pigtail were varied separately. The saturation energy each was adapted for the maximum energy, where the propagation maintained stable versus small perturbations, while the residual fiber and simulation parameters remained constant.

In Fig. 5.15, the resulting maximum pulse energy and B integral are plotted versus the respective mode-field area (MFA). A first result is that although the pulse energy decreases with a smaller MFA inside the NDF, the B integral exceeds 2.15 rad, which

was the maximum in every of the simulations presented above, by nearly a factor 2. Therefore, the accumulated nonlinear phase does not necessarily impose a general upper pulse energy limit as this is regarded to be the case for soliton and stretched-pulse lasers [18].

Furthermore, in both cases, the pulse energy monotonically increased with the MFA, whereat this dependency is more distinct for the TDF. However, along variation of the MFA in the NDF, the B integral decreased with increasing MFA, while for the TDF, a nearly linearly dependency could be observed. Closer investigation reveals that the increase of the B integral with increasing MFA inside the TDF relates to larger nonlinear phase accumulation inside the NDF due to the larger pulse energy, while the contribution of the TDF even reduces. Contrary, the nonlinear phase accumulated inside the TDF remains below about $1/3\,\pi$ along variation of the MFA of the NDF. Therefore it can be concluded that the anomalous dispersion segments and thus mainly the TDF and the following fiber pigtail, where the pulse energy becomes maximal, impose a pulse energy limitation in the observed operation regime.

Pulse parameter optimization

As stated before, a possible approach to adjust the pulse energy is the adaptation of the cavity dispersion, which however includes a trade-off between pulse energy and duration. In the current setup, the nonlinearity of the anomalous dispersion fibers was identified to limit the maximum pulse energy. As the combination of normal GVD and nonlinearity linearizes the pulse chirp and thus could contribute to stabilize the pulse propagation, rearrangement of the fiber segments might be a suitable and relatively simple way to optimize the pulse parameters. In order to investigate the potential of this approach, the NDF was partly shifted between the TDF and the following fiber pigtail. The residual parameters, especially the cavity dispersion, were kept constant in order to maintain the comparability of the results.

In Fig. 5.16 (a), the pulse energy and duration after compression are plotted versus the length of the NDF segment. The pulse duration decreases from about 400 fs to about 250 fs at a length of 2.5 m and slightly increases again with larger length of the NDF.

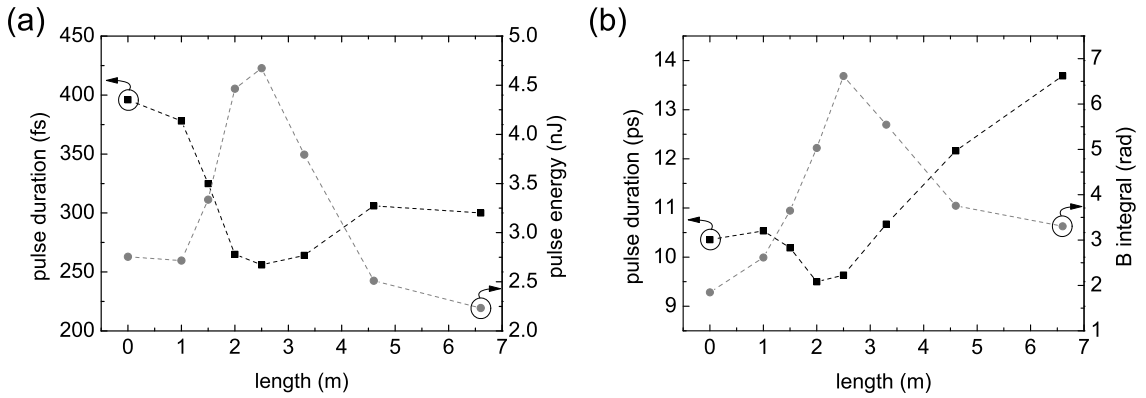

Figure 5.16: (a) Maximum pulse energy (black squares) and pulse duration after compression (grey circles) as well as (b) pulse duration before compression (black squares) and B integral (grey circles) versus length of the shifted NDF segment.

Simultaneously, the pulse energy increases from about 2.8 to 4.5 nJ and reduces again to below 2.5 nJ, when the complete NDF fiber segment is placed behind the TDF.
A similar correlation can be found for the duration of the uncompressed pulse and the B integral (Fig. 5.16 (b)). The pulse duration slightly decreases from about 10.5 ps to a minimum of about 9.5 ps at 2.5 m and significantly increases with increasing fiber length. The B integral corresponding to the short pulse duration and large pulse energy reaches a maximum of more than 2π at 2.5 m and significantly reduces with larger as well as smaller length of the shifted NDF segment.
According to these results, proper arrangement of the fiber sections enables significantly larger pulse energies as well as shorter pulse durations compared to the previous setup. Furthermore, the maximum B integral of more than 2π again verifies that the pulse energy limitation is not imposed by the overall cavity nonlinearity, but also relates to the distribution of specific fiber segments.

5.3 Conclusion

In this chapter, implementation of a fiber providing normal GVD in the 2 µm spectral region into a core-pumped, thulium-doped fiber laser was investigated. The fiber

was used to adapt the pulse parameters of a hybridly mode-locked laser operating in the fundamental soliton regime. Furthermore, a monotonically positively chirped pulse propagation scheme could be achieved. The mode-locked operation was self-starting and remained stable for hours in a laboratory environment. Even if the mode-locking was interrupted due to mechanical disruptions, it usually restored within several seconds.

The soliton laser delivered pulses with a maximum energy of up to 250 pJ, of which about 30 % of the pulse energy were contained in the Kelly-sidebands. Partly compensating for the anomalous fiber GDD laser resulted in a decrease of the pulse duration from 0.51 to 0.47 ps.

With the monotonically positively chirped pulse operation scheme, the laser delivered pulses with about 10 ps duration and a nearly rectangular spectrum, whose width scaled with the pulse energy. A minimum pulse duration of 482 fs after compression with a standard grating compressor could be achieved with a pulse energy of 0.7 nJ. Further increase of the pump power led to a degrading compressibility of the pulses and finally to destabilization of the laser operation. To the best of the author's knowledge, this was the first publication on PCP of a fiber laser in the 2 µm spectral region with the implementation of NDF for dispersion management [52].

The experimentally observed results could well be reproduced using numerical simulations. With these simulations, the conclusions derived from the experimental results could be verified and deeper insight into the pulse evolution inside the resonator could be provided. They furthermore indicate that the pulse energy and spectral width scale with the cavity dispersion. This agrees with previous investigations in the normal dispersion region at 1 µm and therefore indicates that these relation is also valid for PCP fiber lasers in the 2 µm spectral region, in spite of the typically anomalous GVD of amplification fiber.

The nonlinearity of the anomalous GVD fiber section, mainly the amplification fiber and the following pigtail was found to impose a limitation on the maximum pulse energy. The simulations indicate that shifting parts of the NDF segment behind the amplification fiber provides a relatively simple approach to achieve significantly shorter pulse

durations and larger energies. This is attributed to the linearizing influence of the combination of normal GVD and SPM on the spectral chirp of a positively chirped pulse. MI provide a further explanation for the limited pulse energy. However, the sidebands in the experimentally observed pulse spectra, which indicate MI, could not be observed in the numerical simulations. A possible explanation is that the source of the initial fluctuations, which cause the MI, is not included in the simulation model. Hence, the effect actually limiting experimentally achieved pulse energy could not be finally determined.

6 Conclusion

In this thesis, ultrashort pulse thulium fiber oscillators and amplifiers were studied experimentally and numerically. Several concepts, which had been successfully applied in the 1 and 1.5 µm spectral region were transferred to the 2 µm amplification band of thulium-doped fibers and investigated with regard to their similarities and differences.
By implementing a grating arrangement with a telescope for dispersion management, stretched-pulse operation could be achieved in a thulium-doped double-clad fiber laser for the first time. The grating arrangement enabled continuous variation of the cavity group delay dispersion while maintaining mode-locked operation. Dispersion variation in a stretched-pulse fiber laser had previously been investigated with erbium-doped fibers at 1.5 µm [35]. The authors used fibers with alternating dispersion for dispersion management and could vary the cavity dispersion by successively changing the lengths of one of the applied fiber segments with similar results as presented here.
The largest pulse energy of 5.4 nJ could be achieved with slightly positive cavity group delay dispersion, while still a very short pulse duration of about 360 fs could be maintained. Similar output pulse energies have so far only been achieved with an oscillator-amplifier configuration. In 2007, Kivistö et al. achieved a pulse energy of 4.6 nJ by launching pulses from a thulium-holmium-doped fiber oscillator with a duration of about 800 fs and 0.4 nJ energy into a subsequent amplifier [5]. The resulting generation of a Raman soliton led to shortening of the pulse duration down to 150 fs at an emission wavelength of 2.15 µm during amplification.
The variation of the output pulse parameters as a function of pump power was exemplary examined for -0.028 ps^2 and +0.039 ps^2 of cavity dispersion. While for anomalous cavity dispersion, the pump power could only slightly be varied and no significant changes in the output parameters were observed, at normal cavity dispersion the output char-

acteristics strongly depended on the pump power. The variation of the output pulse characteristics were attributed to a shift of the position of minimum pulse duration inside the resonator. A minimum pulse duration of 216 fs after compression with cavity dispersion of $+0.039\,\mathrm{ps}^2$ was achieved.
The experimental results agreed well with theoretical predictions as well as previously reported results and could be reproduced very well by numerical simulations for a wide dispersion range. Deviations of experimental and numerical results were attributed to polarization effects, which were not included in the applied numerical software. The pulse energy was estimated to be limited by the onset of a nonlinear chirp.

In the following, the pulses delivered from the stretched-pulse laser were used to seed a subsequent amplifier using fibers with the same geometry as for the oscillator. By positively prechirping the pulses, significant shortening of the pulse duration during amplification with no subsequent pulse recompression could be achieved. The pulse duration of 97 fs after amplification was even shorter than the results of Imeshev and Fermann, who could achieve pulse shortening from 150 to 108 fs duration during the amplification at a center wavelength of 1980 nm by positively prechirping pulses from a Raman-shifted erbium seed oscillator [11]. However, the maximum pulse energy of 17 nJ and average output power of 644 mW were limited by excessive nonlinear phase at the end of the amplification fiber due to the short pulse duration and high pulse energy, while Imeshev and Fermann achieved a pulse energy of 31 nJ corresponding to 3.1 W of average output power, which was limited by the available pump power.
By applying the chirped pulse amplification scheme, significant pulse energy scaling could be achieved. Due to gain narrowing and a slight mismatch of the center wavelength of the seed and the amplification spectrum, the Fourier-limited pulse duration slightly increased during amplification. Although some influence of nonlinearity on the pulse could be observed, the amplification remained mainly linear and the output power was limited by the available pump power. Hence, at the maximum pulse energy of 151 nJ, corresponding to an average output power of 5.7 W, the pulses could still be compressed

to about 17 % above Fourier-limit. Both the average output power and the single pulse energy represented a record in the amplification of ultrashort pulses with thulium doped fibers at the time of publication.
The reported results represent the first application of the chirped pulse amplification scheme in the 2 µm spectral region. Very recently, several authors reported on linear amplification of pulses with picosecond durations in the 2 µm spectral region. Renard et al. achieved pulses with an energy of 26 nJ and a duration of 3.5 ps at a center wavelength of 1.96 µm in a fiber-integrated master oscillator power amplifier configuration [53]. The pulse energy was limited by the onset of nonlinear effects due to the soliton pulse propagation. With a very similar concept, Liu et al. could achieve an average output power of 20.7 W, corresponding to a pulse energy of 200 nJ and a duration of 18 ps with two cascaded power amplifiers, limited by the available pump power [54]. However, in both publications, a soliton laser with a spectral bandwidth significantly below 2 nm was used as seed source. Therefore, the CPA for a reduction of the peak intensity would be hardly applicable, because very large dispersion values would be required for considerable pulse stretching.

In order to reduce freespace sections and to progress towards an all-fiber integrated system, an oscillator with a core-pumping scheme and a fiber providing normal dispersion in the 2 µm spectral region for dispersion management was set up. With this approach, pulse adaptation of a laser operating in the fundamental soliton regime as well as a monotonically positively chirped pulse propagation scheme could be demonstrated.
The implementation of the hybrid mode-locking scheme in a soliton laser enabled an increase of the extracted pulse energy by more than 50 %. By partly compensating for the anomalous fiber GDD, a simple method for a tuning of the pulse duration could be demonstrated.
With the PCP scheme, the laser provided pulses with 0.7 nJ energy and about 10 ps duration, which could externally be compressed to sub-500 fs using a standard grating compressor. To the best of the author's knowledge, this was the first demonstration

of monotonically positively chirped pulse evolution of a fiber laser in the 2 µm spectral region via the implementation of a normal dispersion fiber for dispersion management. The experimentally observed results could well be reproduced using numerical simulations. With these simulations, the pulse propagation scheme derived from the experimental results and explanation for the pulse energy limitation could be verified and deeper insight into the pulse evolution inside the resonator could be provided. The simulations furthermore indicate that the well-known relation of pulse energy, duration and cavity dispersion is also valid for PCP fiber lasers in the 2 µm spectral region.

By variation of the mode-field diameters of the fiber sections, which mostly contributed to the accumulation of the nonlinear phase, the nonlinearity of the anomalous GVD fiber section was found to impose a limitation on the maximum pulse energy. Rearrangement of the fiber sections provides a relatively simple, but promising approach to achieve significantly shorter pulse durations as well as larger energies.

A similar operation regime in a thulium-holmium-doped fiber oscillator had previously been achieved by Gumenyuk et al. by applying a chirped fiber Bragg grating for dispersion management [51]. Chirped fiber Bragg gratings can easily be integrated as an output coupler in a linear resonator configuration and thus provide a very simple setup. The cavity dispersion can be adjusted by varying the cavity-internal fiber lengths. However, this concept also implies a trade-off between reflectivity and reflection bandwidth of the grating. With the presented setup, a pulse energy of 2.2 nJ with a duration of 11.7 ps could be achieved, limited by the available pump power. A subsequent recompression of the pulses was not performed. By implementing a dispersion compensating fiber into a thulium-doped fiber oscillator Jiang et al. could achieve a minimum pulse duration of 78 fs with 0.28 nJ of pulse energy at a center wavelength of 1.95 µm [55]. However, the authors did not provide any information on the cavity-internal pulse propagation scheme. In a very recent publication, the same group could achieve a pulse duration of 58 fs with 1 nJ of pulse energy directly from a thulium-doped fiber laser with very short fiber lengths and a dispersion compensating fiber operating in the fundamental soliton regime [56].

In conclusion, different approaches for pulse parameter scaling have been investigated. The shortest pulse durations could be observed with a dispersion-managed oscillator operating in the stretched-pulse regime. With a subsequent amplifier, the pulse energy could be significantly increased while maintaining a very short pulse duration. A hybridly mode-locked oscillator with fiber-based dispersion management provides a promising source for further pulse parameter scaling.

7 Outlook

In the last few years, ultra-short pulse thulium doped fiber lasers came into the focus of intensive research and development. Nowadays, q-switched and soliton mode-locked all-fiber integrated lasers are already commercially available and all-fiber configurations with chirped fiber Bragg gratings for dispersion management have successfully been demonstrated. Nevertheless, regarding the monotonically positively chirped pulse operation scheme thulium lasers are still inferior in terms of pulse energy and duration, compared to lasers based on ytterbium and erbium. The numerical investigations in this thesis suggest different approaches to further scale the pulse parameters. However, these results have to be verified experimentally regarding the scalability of the pulse parameters as well as the effect actually limiting the pulse energy. The implementation of a spectral filter is furthermore an aspect, which has not yet been investigated at all. Spectral filtering can additionally stabilize the pulse propagation and therefore provide a further element to adapt the pulse parameters.
Nevertheless, even if the conclusions derived from the numerical results can be experimentally confirmed, the pulse energies achieved with this concept still remain limited. In order to achieve results comparable to the 1 µm spectral region, amplification fibers with normal group delay dispersion are required. With such fibers, the "dissipative soliton"-regime, which is state-of-the-art in ultrashort pulse ytterbium- and erbium-doped lasers, should be applicable to thulium fiber lasers as well and significantly larger pulse energies could be expected. Since thulium-doping in silica fibers is accompanied by a significant increase of the numerical aperture, this should be relatively easily to achieve by a respective design of the fiber's refractive index profile.

Furthermore, the results presented in this thesis show that ultrashort pulses in the 2 µm

spectral region can be efficiently amplified in thulium-doped double-clad fibers with 793 nm diode pumping. Meanwhile, diode lasers with several ten Watt power out of a 100 µm diameter fiber core as well as corresponding fiber couplers are commercially available, which enables robust, high power all fiber-integrated amplifier configurations. Thulium-doped fiber lasers operating with a monotonically positively chirped pulse operation scheme provide an excellent seed source for subsequent amplification towards the Microjoule regime.

Both for generation as well as amplification of ultrashort pulses the combination of normal dispersion and low nonlinearity is favourable as it prevents soliton effects. However, shifting the fiber dispersion towards the normal regime via waveguide dispersion results in small mode-field diameters and therefore in larger nonlinear influence and lower damage thresholds. This conflict could be dissolved by different fiber geometries. Microstructured fibers could possibly provide large mode-field diameters with still normal group velocity dispersion and thus enable even further scaling of the pulse parameters in ultrashort pulse thulium-doped fiber lasers as well as amplifiers.

Furthermore, with the increasing availability of components, the concepts investigated in this thesis can be the transferred to an all fiber-integrated setup enabling further progress towards the spreading of ultra-short pulse thulium fiber lasers in various application areas.

acronyms

AC	autocorrelation
ASE	amplified spontaneous emission
CPA	chirped-pulse amplification
CW	continuous wave
DCM	dichroic mirror
DDL	dispersive delay line
FR	Faraday rotator
FS	free space section
FWHM	full width at half maximum
GDD	group delay dispersion
GVD	group velocity dispersion
HWP	half waveplate
IRS	intrapulse Raman scattering
LMA	large-mode area
MFA	mode-field area
MI	modulation instability
MW	megawatt
NA	numerical aperture
NDF	normal dispersion fiber
NLSE	nonlinear Schrödinger equation
NPE	nonlinear polarization evolution
OSA	optical spectrum analyzer
PMD	polarization mode dispersion
PCP	positively chirped pulse operation

RF	radio-frequency
RMS	root mean square
SAbs	saturable absorber
SBR	saturable Bragg reflector
SeSAM	semiconductor saturable absorber mirror
SMF	single-mode fiber
SOD	second order dispersion
SPM	self-phase modulation
TDF	thulium-doped fiber
TFP	thin-film polarizer
TOD	third order dispersion
QWP	quarter waveplate
WDM	wavelength division multiplexer
XPM	cross-phase modulation

Bibliography

[1] K. Tamura, E. P. Ippen, H. A. Haus, and L. E. Nelson, *77-fs pulse generation from a stretched-pulse mode-locked all-fiber ring laser*, Opt. Lett. **18**, 1080 (1993).

[2] F. O. Ilday, J. R. Buckley, H. Lim, F. W. Wise, and W. G. Clark, *Generation of 50-fs, 5-nJ pulses at 1.03 μm from a wave-breaking-free fiber laser*, Opt. Lett. **28**, 1365–1367 (2003).

[3] L. E. Nelson, E. P. Ippen, and H. A. Haus, *Broadly tunable sub-500 fs pulses from an additive-pulse mode-locked thulium-doped fiber ring laser*, Applied Physics Letters **67**, 19–21 (1995).

[4] R. C. Sharp, D. E. Spock, N. Pan, and J. Elliot, *190-fs passively mode-locked thulium fiber laser with a low threshold*, Opt. Lett. **21**, 881 (1996).

[5] S. Kivistoe, T. Hakulinen, M. Guina, and O. G. Okhotnikov, *Tunable Raman soliton source using mode-locked Tm-Ho fiber laser*, IEEE Photonics Technology Letters **19**, 934–936 (2007).

[6] M. Solodyankin, E. Obraztsova, A. Lobach, A. Chernov, A. Tausenev, V. Konov, and E. Dianov, *1.93 μm mode-locked thulium fiber laser with a carbon nanotube absorber*, Opt. Express **33**, 1336–1338 (2008).

[7] W. B. Cho, A. Schmidt, J. H. Yim, S. Y. Choi, S. Lee, F. Rotermund, U. Griebner, G. Steinmeyer, V. Petrov, X. Mateos, M. C. Pujol, J. J. Carvajal, M. Aguiló, and F. Díaz, *Passive mode-locking of a Tm-doped bulk laser near 2 μm using a carbon nanotube saturable absorber*, Opt. Express **17**, 11007–11012 (2009).

[8] A. A. Lagatsky, F. Fusari, S. Calvez, S. V. Kurilchik, V. E. Kisel, N. V. Kuleshov, M. D. Dawson, C. T. A. Brown, and W. Sibbett, *Femtosecond pulse operation of a Tm,Ho-codoped crystalline laser near 2 μm*, Opt. Lett. **35**, 172–174 (2010).

[9] A. Lagatsky, S. Calvez, J. A. Gupta, V. E. Kisel, N. V. Kuleshov, C. T. A. Brown, M. D. Dawson, and W. Sibbett, *Broadly tunable femtosecond mode-locking in a Tm:KYW laser near 2 um*, Opt. Express **19**, 9995–10000 (2011).

[10] A. A. Lagatsky, P. Koopmann, P. Fuhrberg, G. Huber, C. T. A. Brown, and W. Sibbett, *Passively mode locked femtosecond Tm:Sc2O3 laser at 2.1 μm*, Opt. Lett. **37**, 437–439 (2012).

[11] G. Imeshev and M. E. Fermann, *230-kW peak power femtosecond pulses from a high power tunable source based on amplification in Tm-doped fiber*, Optics Express **13**, 7424–7431 (2005).

[12] S. Jackson and T. King, *Theoretical modeling of Tm-doped silica fiber lasers*, Journal of Lightwave Technology **17**, 948–956 (1999).

[13] J. Wu, Z. Yao, J. Zong, and S. Jiang, *Highly efficient high-power thulium-doped germanate glass fiber laser*, Optics Letters **32**, 638–640 (2007).

[14] D. C. Hanna, R. M. Percival, R. G. Smart, and A. C. Tropper, *Efficient and tunable operation of a Tm-doped fibre laser*, Optics Communications **75**, 283–286 (1990).

[15] M. Engelbrecht, F. Haxsen, D. Wandt, and D. Kracht, *Wavelength resolved intracavity measurement of the cross sections of a Tm-doped fiber*, Opt. Express **16**, 1610–1615 (2008).

[16] G. P. Agrawal, *Nonlinear Fiber Optics* (Academic Press, 2001), 3rd ed.

[17] K. Tai, A. Hasegawa, and A. Tomita, *Observation of modulational instability in optical fibers*, Phys. Rev. Lett. **56**, 135–138 (1986).

[18] F. W. Wise, A. Chong, and W. H. Renninger, *High-energy femtosecond fiber lasers based on pulse propagation at normal dispersion*, Laser & Photon **2**, 58–73 (2008).

[19] S. Kelly, *Characteristic sideband instability of periodically amplified average soliton*, Electronics Letters **28**, 806–807 (1992).

[20] K. Kieu, W. H. Renninger, A. Chong, and F. W. Wise, *Sub-100 fs pulses at watt-level powers from a dissipative-soliton fiber laser*, Opt. Lett. **34**, 593–595 (2009).

[21] K. R. Tamura, *Additive Pulse Mode-Locked Erbium-Doped Fiber Lasers*, Ph.D. thesis, Massachusetts Institute of Technology (1994).

[22] L. E. Nelson, D. J. Jones, K. Tamura, H. A. Haus, and E. P. Ippen, *Ultrashort-pulse fiber ring lasers*, Applied Physics B: Lasers and Optics **65**, 277–294 (1997).

[23] D. Anderson, M. Desaix, M. Karlsson, M. Lisak, and M. L. Quiroga-Teixeiro, *Wave-breaking-free pulses in nonlinear-optical fibers*, J. Opt. Soc. Am. B **10**, 1185–1190 (1993).

[24] W. Renninger, A. Chong, and F. Wise, *Pulse Shaping and Evolution in Normal-Dispersion Mode-Locked Fiber Lasers*, IEEE Journal of Selected Topics in Quantum Electronics **18**, 389 –398 (2012).

[25] B. G. Bale, S. Boscolo, and S. K. Turitsyn, *Dissipative dispersion-managed solitons in mode-locked lasers*, Opt. Lett. **34**, 3286–3288 (2009).

[26] H. Haus, *Parameter ranges for CW passive mode locking*, IEEE Journal of Quantum Electronics **12**, 169–176 (1976).

[27] M. Haiml, R. Grange, and U. Keller, *Optical characterization of semiconductor saturable absorbers*, Applied Physics B - Lasers and Optics **79**, 331–339 (2004).

[28] E. P. Ippen, *Principles of passive mode locking*, Applied Physics B Photophysics Laser Chemistry **58**, 159–170 (1994).

[29] K. Tamura, J. Jacobson, E. P. Ippen, H. A. Haus, and J. G. Fujimoto, *Unidirectional ring resonators for self-starting passively mode-locked lasers*, Opt. Lett. **18**, 220 (1993).

[30] O. E. Martinez, J. P. Gordon, and R. L. Fork, *Negative group-velocity dispersion using refraction*, J. Opt. Soc. Am. A **1**, 1003 (1984).

[31] T. Schreiber, *FiberDesk*, website: http://www.fiberdesk.com.

[32] T. Pfeiffer and H. Buelow, *Analytical gain equation for erbium-doped fiber amplifiers including mode field profiles and dopant distribution*, IEEE Photonics Technology Letters **4**, 449–451 (1992).

[33] D. Marcuse, *Loss analysis of single-mode fiber splices*, Bell System Technical Journal **56**, 703–718 (1977).

[34] H. Haus, K. Tamura, L. Nelson, and E. Ippen, *Stretched-pulse additive pulse mode-locking in fiber ring lasers: theory and experiment*, IEEE Journal of Quantum Electronics **31**, 591–598 (1995).

[35] K. Tamura, L. E. Nelson, H. A. Haus, and E. P. Ippen, *Soliton versus nonsoliton operation of fiber ring lasers*, Applied Physics Letters **64**, 149–151 (1994).

[36] D. Anderson, M. Desaix, M. Lisak, and M. L. Quiroga-Teixeiro, *Wave breaking in nonlinear-optical fibers*, J. Opt. Soc. Am. B **9**, 1358–1361 (1992).

[37] D. Strickland and G. Mourou, *Compression of amplified chirped optical pulses*, Optics Communications **56**, 219–221 (1985).

[38] S. D. Jackson, *Cross relaxation and energy transfer upconversion processes relevant to the functioning of 2 μm Tm^{3+}-doped silica fibre lasers*, Optics Communications **230**, 197–203 (2004).

[39] D. Gloge, *Dispersion in Weakly Guiding Fibers*, Appl. Opt. **10**, 2442–2445 (1971).

[40] J. A. Curcio and C. C. Petty, *The Near Infrared Absorption Spectrum of Liquid Water*, J. Opt. Soc. Am. **41**, 302–304 (1951).

[41] N. Akhmediev, J. Soto-Crespo, and P. Grelu, *Roadmap to ultra-short record high-energy pulses out of laser oscillators*, Physics Letters A **372**, 3124 – 3128 (2008).

[42] J. Buckley, A. Chong, S. Zhou, W. Renninger, and F. W. Wise, *Stabilization of high-energy femtosecond ytterbium fiber lasers by use of a frequency filter*, J. Opt. Soc. Am. B **24**, 1803–1806 (2007).

[43] N. J. Smith, N. J. Doran, F. M. Knox, and W. Forysiak, *Energy-scaling characteristics of solitons in strongly dispersion-managed fibers*, Opt. Lett. **21**, 1981–1983 (1996).

[44] M. Droques, A. Kudlinski, G. Bouwmans, G. Martinelli, L. Bigot, and A. Mussot, *Demonstration of Modulation Instability Assisted by a Periodic Dispersion Landscape in an Optical Fiber*, in "CLEO: Science and Innovations," (Optical Society of America, 2012), p. CTh4B.7.

[45] P. Kaewplung, T. Angkaew, and K. Kikuchi, *Complete Analysis of Sideband Instability in Chain of Periodic Dispersion-Managed Fiber Link and Its Effect on Higher Order Dispersion-Managed Long-Haul Wavelength-Division Multiplexed Systems*, J. Lightwave Technol. **20**, 1895 (2002).

[46] S. Coen and M. Haelterman, *Modulational Instability Induced by Cavity Boundary Conditions in a Normally Dispersive Optical Fiber*, Phys. Rev. Lett. **79**, 4139–4142 (1997).

[47] J. Peng, L. Zhan, Z. Gu, J. Liu, S. Luo, X. Shen, and Q. Shen, *Modulation Instability in Dissipative Soliton Fiber Lasers and Its Application on Cavity Net Dispersion Measurement*, Journal of Lightwave Technology **30**, 2707 –2712 (2012).

[48] A. Chong, W. H. Renninger, and F. W. Wise, *Properties of normal-dispersion femtosecond fiber lasers*, J. Opt. Soc. Am. B **25**, 140–148 (2008).

[49] H. A. Haus, J. G. Fujimoto, and E. P. Ippen, *Structures for additive pulse mode locking*, J. Opt. Soc. Am. B **8**, 2068 (1991).

[50] A. Wienke, F. Haxsen, D. Wandt, U. Morgner, J. Neumann, and D. Kracht, *Ultrafast, stretched-pulse thulium-doped fiber laser with a fiber-based dispersion management*, Opt. Lett. **37**, 2466–2468 (2012).

[51] R. Gumenyuk, I. Vartiainen, H. Tuovinen, and O. G. Okhotnikov, *Dissipative dispersion-managed soliton 2 μm thulium/holmium fiber laser*, Opt. Lett. **36**, 609–611 (2011).

[52] F. Haxsen, D. Wandt, U. Morgner, J. Neumann, and D. Kracht, *Monotonically chirped pulse evolution in an ultrashort pulse thulium-doped fiber laser*, Opt. Lett. **37**, 1014–1016 (2012).

[53] W. Renard, G. Canat, and P. Bourdon, *26 nJ picosecond solitons from thulium-doped single-mode master oscillator power fiber amplifier*, Opt. Lett. **37**, 377–379 (2012).

[54] J. Liu, Q. Wang, and P. Wang, *High average power picosecond pulse generation from a thulium-doped all-fiber MOPA system*, Opt. Express **20**, 22442–22447 (2012).

[55] J. Jiang, C. Mohr, J. Bethge, M. Fermann, and I. Hartl, *Fully Stabilized, Self-Referenced Thulium Fiber Frequency Comb*, in "CLEO/Europe and EQEC 2011 Conference Digest," (Optical Society of America, 2011), p. PDB1.

[56] J. Jiang, C. Mohr, J. Bethge, A. Mills, W. Mefford, I. Hartl, and M. E. Fermann, *500 MHz, 58fs highly coherent Tm fiber soliton laser*, in "Conference on Lasers and Electro-Optics," (2012), p. CTh5D.7.

Publications in Peer-Reviewed Journals

[57] M. Engelbrecht, F. Haxsen, D. Wandt, and D. Kracht, *Wavelength resolved intracavity measurement of the cross sections of a Tm-doped fiber*, Opt. Express **16**, 1610–1615 (2008).

[58] M. Engelbrecht, F. Haxsen, A. Ruehl, D. Wandt, and D. Kracht, *Ultrafast thulium-doped fiber-oscillator with pulse energy of 4.3 nJ*, Opt. Lett. **33**, 690–692 (2008).

[59] F. Haxsen, A. Ruehl, M. Engelbrecht, D. Wandt, U. Morgner, and D. Kracht, *Stretched-pulse operation of a thulium-doped fiber laser*, Opt. Express **16**, 20471–20476 (2008).

[60] F. Haxsen, D. Wandt, U. Morgner, J. Neumann, and D. Kracht, *Pulse characteristics of a passively mode-locked thulium fiber laser with positive and negative cavity dispersion*, Opt. Express **18**, 18981–18988 (2010).

[61] F. Haxsen, D. Wandt, U. Morgner, J. Neumann, and D. Kracht, *Pulse energy of 151 nJ from ultrafast thulium-doped chirped-pulse fiber amplifier*, Opt. Lett. **35**, 2991–2993 (2010).

[62] F. Haxsen, D. Wandt, U. Morgner, J. Neumann, and D. Kracht, *Monotonically chirped pulse evolution in an ultrashort pulse thulium-doped fiber laser*, Opt. Lett. **37**, 1014–1016 (2012).

[63] A. Wienke, F. Haxsen, D. Wandt, U. Morgner, J. Neumann, and D. Kracht, *Ultrafast, stretched-pulse thulium-doped fiber laser with a fiber-based dispersion management*, Opt. Lett. **37**, 2466–2468 (2012).

Publications in Conference Proceedings

[64] M. Engelbrecht, F. Haxsen, A. Ruehl, D. Wandt, and D. Kracht, *320-fs Thulium-Doped Fiber-Ring-Laser with a Pulse Energy of 3.5-nJ*, in "Conference on Lasers and Electro-Optics," (Optical Society of America, 2008), p. CFD4.

[65] F. Haxsen, M. Engelbrecht, D. Wandt, and D. Kracht, *Passiv modengekoppelter Thulium-dotierter Faserlaser mit 3,45 nJ Pulsenergie*, in "DPG Frühjahrstagung," (Deutsche Physikalische Gesellschaft e.V., 2008), p. Q 46.1.

[66] F. Haxsen, M. Engelbrecht, A. Ruehl, D. Wandt, U. Morgner, and D. Kracht, *High-power passively mode-locked thulium-doped fibre ring laser with variable dispersion compensation*, in "Europhoton Conference," (European Physical Society, 2008), p. TUoD.4.

[67] F. Haxsen, D. Wandt, U. Morgner, D. Kracht, and J. Neumann, *Pulsdynamik in einem fs Thulium-Faserlaser*, in "DPG Frühjahrstagung," (Deutsche Physikalische Gesellschaft e.V., 2010), p. TuB5.

[68] F. Haxsen, D. Wandt, U. Morgner, D. Kracht, and J. Neumann, *Dispersion Variation of a Thulium-Doped Stretched-Pulse Fiber Laser with Spectral Filtering*, in "Conference on Lasers and Electro-Optics," (Optical Society of America, 2010), p. CMW3.

[69] F. Haxsen, D. Wandt, D. Kracht, J. Neumann, and U. Morgner, *Chirped-pulse Amplification of an Ultrashort Pulse Thulium Fiber Laser*, in "Europhoton Conference," (European Physical Society, 2010), p. TuB5.

[70] F. Haxsen, D. Wandt, U. Morgner, J. Neumann, and D. Kracht, *Hybrid mode-locked*

thulium soliton fiber laser, in "IEEE Photonics Conference," (Institute of Electrical and Electronics Engineers, 2011), pp. 885 – 886.

[71] A. Wienke, F. Haxsen, D. Wandt, U. Morgner, J. Neumann, and D. Kracht, *Fiber based dispersion management in an ultrafast thulium-doped fiber laser and external compression with a normal dispersive fiber*, in "Advanced Solid-State Photonics," (Optical Society of America, 2012), p. AT4A.26.

[72] F. Haxsen, D. Wandt, U. Morgner, J. Neumann, and D. Kracht, *Positively chirped pulse evolution in a passively mode-locked thulium-doped fiber laser*, in "Advanced Solid-State Photonics," (Optical Society of America, 2012), p. AM4A.24.

[73] A. Wienke, F. Haxsen, D. Wandt, U. Morgner, J. Neumann, and D. Kracht, *Dispersion management with a normal dispersive fiber in an ultrafast thulium-doped fiber laser*, in "Photonics Europe," (International Society for Optical Engineering, 2012), pp. 8433–13.

[74] F. Haxsen, D. Wandt, U. Morgner, J. Neumann, and D. Kracht, *Positively chirped pulses from a mode-locked thulium fiber laser*, in "Photonics Europe," (International Society for Optical Engineering, 2012), pp. 8433–17.

[75] A. Wienke, F. Haxsen, D. Wandt, U. Morgner, J. Neumann, and D. Kracht, *Stretched-pulse operation of a thulium-doped fiber laser with a fiber-based dispersion management*, "Conference on Lasers and Electro-Optics," (Optical Society of America, 2012), p. CM1B.7.

[76] F. Haxsen, D. Wandt, U. Morgner, J. Neumann, and D. Kracht, *Positively Chirped Pulses in a Mode-Locked Thulium Fiber Laser - Simulation and Experiment*, "Conference on Lasers and Electro-Optics," (Optical Society of America, 2012), p. CTu1I.2.

Curriculum Vitae

Personal Data

Name:	Frithjof Haxsen
Date of birth:	December 16$^{\text{th}}$ 1982
Place of birth:	Hannover
Nationality:	German

Education

1989 – 1993	Grundschule Hämelerwald
1993 – 1995	Orientierungsstufe Lehrte Ost
1995 – 2002	Gymnasium Lehrte
06/2002	Abitur

University Education

10/2002 – 07/2008	Technical Physics at Leibniz Universität Hannover
07/2008	Degree "Diplom Physiker", Title of the thesis: "Durchstimmbarer kontinuierlich emittierender und passiv modengekoppelter Thulium-Faserlaser"

Professional Affiliations

08/2007 – 10/2007	Practical training at Rowiak GmbH, Hannover
04/2006 – 07/2006	Research assistant at the Institute of Quantum Optics, Leibniz Universität Hannover
10/2006 – 04/2007	Research assistant at Laser Zentrum Hannover e.V., Laser Development Department, Ultrafast Photonics Group
08/2008 – present	Research scientist at Laser Zentrum Hannover e.V., Laser Development Department, Ultrafast Photonics Group

Danksagung

An dieser Stelle möchte ich mich bei denen bedanken, die direkt oder indirekt zum Gelingen dieser Arbeit beigetragen haben, auch wenn dabei nicht alle explizit erwähnt werden können.

Zunächst bedanke ich mich bei Prof. Uwe Morgner für die Betreuung und Begutachtung meiner Arbeit. Weiterhin gilt mein Dank Prof. Detlev Ristau für die Übernahme des Korreferats und Prof. Rolf Haug für die Übernahme des Prüfungsvorsitzes.

Dr. Dietmar Kracht danke ich für die Möglichkeit, meine Arbeiten am Laser Zentrum Hannover e.V. (LZH) durchführen zu können, sowie der logistischen Unterstützung bei der einen oder anderen Konferenz in Übersee.
Bei Dr. Jörg Neumann und Dr. Dieter Wandt bedanke ich mich für die weitestgehende Freiheit in der Gestaltung meiner Forschungsaktivitäten, die gute Unterstützung und die Korrektur dieser Arbeit, die sehr zu ihrem Gelingen beigetragen haben. Weiterhin gilt mein Dank der gesamten Entwicklungsabteilung des LZH für die angenehme Arbeitsatmosphäre, hohe Diskussionsbereitschaft und gute Zusammenarbeit.

Mein Dank gilt ausserdem allen Beteiligten, die zum Zustandekommen des Exzellenzclusters "Centre for Quantum Engineering and Space-Time Research" (QUEST) beigetragen haben, in dessen Rahmen diese Arbeiten durchgeführt wurden.

Zudem danke ich meinen Eltern Katharina und Gerhard Haxsen, die mir auch über Zeit des Studiums hinaus immer mit Rat und Tat zur Seite gestanden haben. Ein besonderer Dank gilt außerdem meiner Freundin Charlotte Schrimpff, die mir in den letzten Jahren auch und vor allem außerhalb meiner Arbeit eine schöne Zeit beschert hat.